Unrest in Long Valley Caldera, California, 1978–2004

DAVID P. HILL

US Geological Survey, 345 Middlefield Rd., Menlo Park, CA 94025, USA
(e-mail: hill@usgs.gov)

Abstract: Long Valley Caldera and the Mono–Inyo Domes volcanic field in eastern California lie in a left-stepping offset along the eastern escarpment of the Sierra Nevada, at the northern end of the Owens Valley and the western margin of the Basin and Range Province. Over the last 4 Ma, this volcanic field has produced multiple volcanic eruptions, including the caldera-forming eruption at 760 000 a BP and the recent Mono–Inyo Domes eruptions 500–660 a BP and 250 a BP. Beginning in the late 1970s, the caldera entered a sustained period of unrest that persisted through the end of the century without culminating in an eruption. The unrest has included recurring earthquake swarms; tumescence of the resurgent dome by nearly 80 cm; the onset of diffuse magmatic carbon dioxide emissions around the flanks of Mammoth Mountain on the southwest margin of the caldera; and other indicators of magma transport at mid- to upper-crustal depths. Although we have made substantial progress in understanding the processes driving this unrest, many key questions remain, including the distribution, size, and relation between magma bodies within the mid-to-upper crust beneath the caldera, Mammoth Mountain, and the Inyo Mono volcanic chain, and how these magma bodies are connected to the roots of the magmatic system in the lower crust or upper mantle.

Long Valley Caldera in eastern California is one of several large calderas around the world that have shown pronounced unrest in the last three decades. In each case, caldera unrest has included recurring earthquake swarms and deformation of the caldera floor by decimetres to metres. In some calderas, the unrest has also included combinations of long-period (LP) and very-long-period (VLP) volcanic earthquakes, elevated efflux of magmatic gases, and changes in the local hydrological system. The unrest in Long Valley Caldera over the past 26 years has included all of the above, with – as yet – no eruption. Within the resort communities of eastern California, reactions to the long-lived unrest and its implications for volcanic hazards are documented elsewhere (Hill 1998; Hill *et al.* 2002*a*). Here, we focus on the evolution of the unrest and its relation to regional tectonic and magmatic processes.

Long Valley Caldera is the largest structure in the Long Valley Caldera–Mono Craters volcanic field that includes Mammoth Mountain and the Mono–Inyo volcanic chain. The caldera appears as an elliptically shaped, 15- by 30-km topographic depression at the base of the steep eastern slope of the Sierra Nevada (Fig. 1). Mammoth Mountain, a 57-ka-old dacitic volcano and the largest ski area in California, stands on the southwest rim of the caldera. The Mono–Inyo volcanic chain is a 40-km-long chain of post-40-ka rhyolitic volcanic centres that extends northward from the west-central part of the caldera to Mono Lake.

Tectonic setting

The Long Valley Caldera–Mono Craters volcanic field resides in a left-stepping offset in the eastern escarpment of the Sierra Nevada at the north end of the Owens Valley graben (Fig. 1). The large, east dipping normal faults that form the eastern escarpment of the Sierra Nevada, mark the western margin of the extensional Basin and Range Province.

Pliocene-to-Recent volcanism in east-central California and the Owens Valley graben to the south is associated with the Eastern California Shear Zone (ECSZ), a zone of active transtensional deformation along the western margin of the Basin and Range Province. The coupled tectonic and magmatic processes within the ECSZ and its extension to the north along the Walker Lane (WL) in western Nevada, reflect the combined influence of dextral slip along the San Andreas Fault transform boundary between the Pacific Plate and North American plates and the westward extension of the crust across the Basin and Range Province. Distributed dextral slip across the transtensional, NNW-striking ECSZ–WL corridor accommodates between 15 to 25% of the relative Pacific–North American plate motion (Dixon *et al.* 2000). Magmatic processes and volcanism within this zone are

From: TROISE, C., DE NATALE, G. & KILBURN, C. R. J. (eds) 2006. *Mechanisms of Activity and Unrest at Large Calderas*. Geological Society, London, Special Publications, **269**, 1–24.
0305-8719/06/$15.00

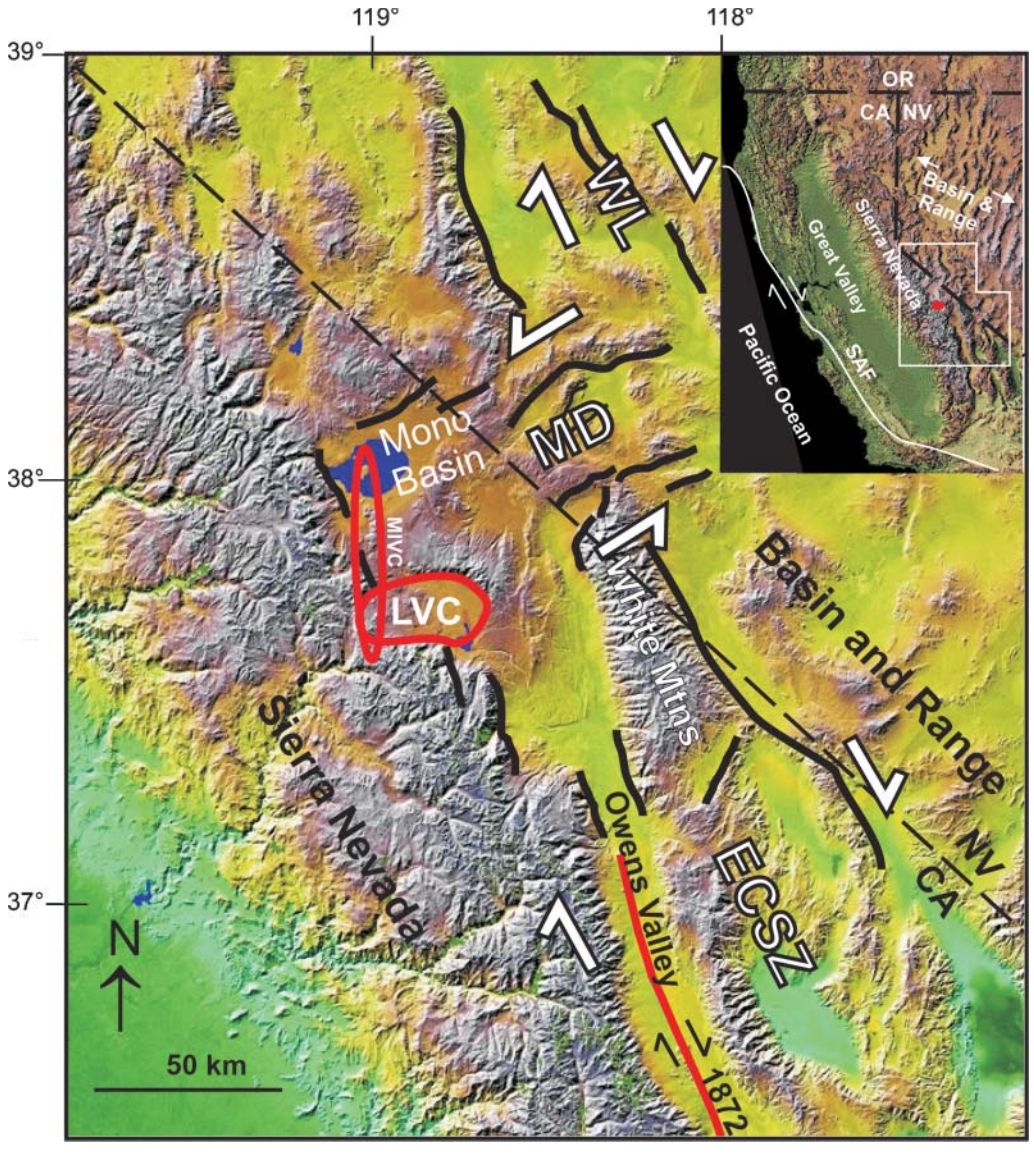

Fig. 1. Shaded relief map of east-central California and western Nevada, showing the location of Long Valley Caldera (LVC) and the Mono–Inyo volcanic chain (MIVC) outlined by red ovals. Increasing elevation is indicated by colours ranging from dark green (at approximately sea-level) to light grey (> 2400 m with maximum elevations reaching *c*. 4300 m). The transition from yellow-green to brown marks the 1700 m contour. Heavy black lines indicate major Quaternary faults. The red line in the Owens Valley indicates surface rupture from the $M \approx 7.6$ Owens Valley earthquake of 1872. White arrows indicate the sense of displacement across the Eastern California Shear Zone (ECSZ), the Mina Deflection (MD), and the Walker Lane (WL). The white outline in the inset shows the map location with respect to the San Andreas Fault (SAF) in coastal California (CA) and the Basin and Range Province in western Nevada (NV) with opposing white arrows indicating the sense of extension. Long Valley Caldera is marked by the small red oval.

generally attributed to the upwelling of magma into the crust from the underlying asthenosphere as the crust stretches, thins and occasionally fractures in response to transtensional extension across the Eastern California shear zone–Walker Lane corridor.

Tectonic elements reflecting the localization of volcanism in the Long Valley Caldera–Mono Craters volcanic field over the past 4 Ma include: (1) the 100-km-wide topographic swell centred on the Mono Basin and characterized by basin elevations systematically exceeding 1750 m, and (2) the Mina Deflection (MD), a zone of northeast-trending sinistral faults that form a right-stepping, dilatational jog in the dextral ECSZ–WL fault system (Fig. 1). Kinematically, distributed sinistral shear across the Mina Deflection implies extension beneath the western margin of the Mono Basin that increases southward in the direction of Long Valley Caldera. The Mono Basin topographic swell is reminiscent of the much broader topographic swell associated with the Yellowstone Caldera and hot spot (Smith & Braile 1994), and is consistent with its being supported by a buoyant volume of elevated temperatures somewhere in the mid-to-lower crust or upper mantle. As of mid-2005, however, the structure of the underlying crust and upper mantle remains poorly resolved, and we can only speculate on the nature of the roots to the Long Valley–Mono Craters volcanic field and the dynamics that have served to focus magmatism in this particular crustal volume.

Volcanic history

The Long Valley Caldera–Mono Craters volcanic field has been a persistent source of volcanic activity throughout the Quaternary (Bailey *et al.* 1976; Bailey 2004; Hildreth 2004). Volcanism in the area began about 4 Ma ago with widespread eruptions of intermediate and basaltic lavas accompanying the onset of large-scale normal faulting and formation of the Owens Valley graben and the eastern front of the Sierra Nevada. Beginning about 2 Ma ago, multiple rhyolitic eruptions from vents along the northeast rim of the present-day caldera formed the Glass Mountain complex (Fig. 2). Long Valley Caldera was formed 760 ka ago by the massive eruption of more than 600 km^3 of rhyolitic lavas (the Bishop Tuff), accompanied by subsidence of a 15- by 30-km elliptical crustal block by 1 to 2 km as the underlying magma chamber was partially evacuated. Smaller eruptions from the residual magma chamber accompanied uplift of the west central section of the caldera over the next 100 000 years to form the resurgent dome. Subsequent eruptions of rhyolite lavas occurred around the margin of the resurgent dome at 500 ka, 300 ka and 100 ka ago (Bailey *et al.* 1976; Bailey 2004).

About 160 ka ago, basaltic lavas began erupting from scattered, monogenetic vents to the west and southwest of the caldera ring-fracture system. These mafic eruptions include the *c.* 100-ka Devil's Postpile flows and, most recently, the 8-ka Red Cones cinder cones and flows. Between 110 ka and 56 ka ago, repeated rhyodacitic eruptions from tightly clustered vents within this mafic field produced the domes and flows that form Mammoth Mountain, which is centred on the southwestern topographic rim of the caldera (Bailey 2004). This mafic volcanic field and the Mammoth Mountain rhyodacites were fed by a distinct magmatic system located outboard of the caldera ring-fracture system (Hildreth 2004).

Rhyolitic eruptions, which began along the Mono–Inyo Domes volcanic chain about 40 ka ago, have continued through to recent times with eruptions along the north end of the Mono Domes about 600 years ago (Bursik & Sieh 1989) and along the south end of the Inyo Domes about 550 years ago (Miller 1985). In both cases, the eruptions resulted from the intrusion of an 8–10-km-long, north-striking feeder dyke into the shallow crust, which vented at several places along strike. Intrusion of a shallow crypto-dome beneath Mono Lake *c.* 250 years ago, uplifted the lake-bottom sediments to form Pahoa Island and vented in a small eruption of andesitic lavas from vents on the north side of the island (Bursik & Sieh 1989). The eruptive history of the Mono–Inyo volcanic chain over the past 5000 years includes some 20 small eruptions (erupted volumes <0.1 km^3) at intervals ranging from 250 to 700 years. Hildreth (2004) suggests that the general migration of volcanism over the past 2 Ma from the Glass Mountain Complex westward to Mammoth Mountain and the Mono–Inyo volcanic chain indicates that the Long Valley Caldera magmatic system is waning, while the Mammoth Mountain–Inyo Domes system is waxing.

Caldera unrest

The region south of Long Valley Caldera that includes the eastern Sierra Nevada and Owens Valley has been one of the most persistent sources of moderate to strong earthquakes in California in historical times, which date from the 1860s in eastern California (Fig. 3, Ellsworth 1990). The northern end of the rupture zone of the great (moment-magnitude $M \approx 7.6$) Owens Valley earthquake of 1872 extended to within 60 km of the caldera (Figs 1 & 3). From 1889

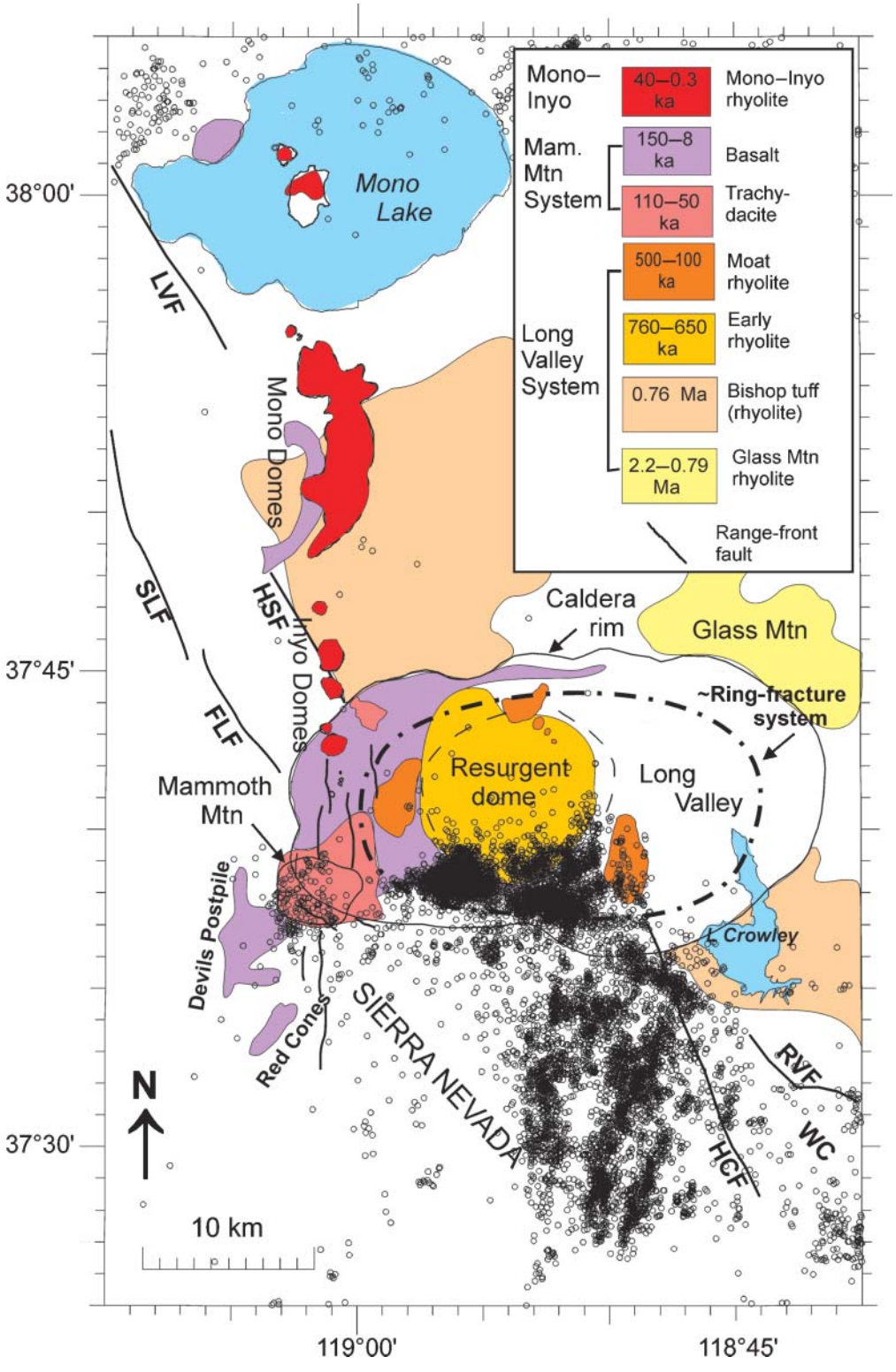
Mono–Inyo
40–0.3 ka
Mono–Inyo rhyolite
Mam. Mtn System
150–8 ka
Basalt
110–50 ka
Trachy-dacite
Long Valley System
500–100 ka
Moat rhyolite
760–650 ka
Early rhyolite
0.76 Ma
Bishop tuff (rhyolite)
2.2–0.79 Ma
Glass Mtn rhyolite
Range-front fault
Mono Lake
LVF
Mono Domes
SLF
HSF
Inyo Domes
FLF
Caldera rim
Glass Mtn
~Ring-fracture system
Resurgent dome
Long Valley
Mammoth Mtn
Devils Postpile
Red Cones
SIERRA NEVADA
Crowley
RVF
WC
HCF
N
10 km
38°00'
37°45'
37°30'
119°00'
118°45'

through to 1970, three $M>6$ earthquakes (Fig. 3) and some 20 $M>5$ earthquakes occurred within 50 km of the south margin of Long Valley Caldera, including a cluster of four $M\geq 5$ events and one $M\approx 6$ event in September 1941 along the Sierra Nevada escarpment *c*. 10 km southeast of the caldera (see Cramer & Toppozada 1980; Ellsworth 1990). (Note: unless noted otherwise, M is local or 'preferred' earthquake magnitude as listed in the Northern California Seismic Network archive.)

None of the $M>5$ earthquakes prior to 1970, however, were located within the caldera. The same appears to be true for $M>3$ earthquakes as far back as the 1940s, when the evolving regional seismic networks operated by the California Institute of Technology and the University of California at Berkeley became capable of detecting and locating $M>3$ earthquakes in eastern California. Van Wormer & Ryall (1980) document an interval of relative seismic quiescence in the eastern Sierra from 1976 through mid-1978 that was interrupted by an $M=5.8$ earthquake on 4 October 1978, located beneath Wheeler Crest (WC in Figs 2 & 3a), *c*. 15 km southeast of the caldera. This earthquake marked the onset of increasing activity within the adjacent Sierra Nevada, the caldera to the north, and Mammoth Mountain on the southwest rim of the caldera, that persisted through the first few years of the twenty-first century. The late-twentieth century surge in activity in Long Valley Caldera and vicinity is thus unique in the short (*c*. 160-year) written history of eastern California.

Increasing unrest: 1978–1983

Following the $M=5.8$ Wheeler Crest earthquake, a series of $M=3$ to 4 earthquakes occurred intermittently within the Sierra Nevada block south of the caldera, within the south moat of the caldera, and beneath the south flank of Mammoth Mountain. This activity culminated in an intense earthquake sequence that began in late May 1980 and then gradually slowed through the summer. The late-May activity included four $M\approx 6$ earthquakes (Hill *et al.* 1985). Three occurred on 25 May; the first located just west of Convict Lake near the south margin of the caldera; the second beneath the south moat (SMSZ), and the third within the Sierra Nevada block about 5 km south of the caldera (Fig. 4). On 27 May 1980, the fourth $M\approx 6$ earthquake struck an area about 10 km south of the caldera (Figs 4 & 5). The vigorous set of aftershocks to this sequence of four $M6$ earthquakes included $M=5.1$, 5.5 and 5.3 earthquakes on 29 June, 1 August and 7 September, respectively.

The focal mechanisms of the four May-1980, $M\approx 6$ earthquakes had dominantly strike-slip solutions with T-axes (extension directions) having a NE–SW orientation generally consistent with right-lateral slip within the WNW-trending SMSZ and left-lateral slip in the NNE-trending seismicity lineations in the adjacent Sierra Nevada block. This basic kinematic pattern with a NE–SW extension direction has prevailed for earthquakes in the caldera and the adjacent Sierra Nevada block through to the present.

The great majority of earthquakes in this 1980 sequence, as well as subsequent unrest episodes, have the appearance of ordinary shear-failure earthquakes with double-couple focal mechanisms. An important subset, however, have characteristics commonly associated with volcanic areas, including non-double-couple focal mechanisms and band-limited frequency content typical of long-period (LP) volcanic and very-long-period (VLP) earthquakes. Moment tensors for two of the May-1980 $M=6$ earthquakes (the northernmost and southernmost in the Sierra Nevada block), for example, as well as the $M=5.8$ earthquake of October 1978, included significant non-double-couple components consistent with either fluid injection or simultaneous shear failure on fault segments at oblique angles to one another (Fig. 3a, Wallace *et al.* 1982; Chouet & Julian 1985; Julian & Sipkin 1985). Prejean *et al.* (2002) see evidence favouring the latter in the structures defined by their high-resolution hypocentre relocations of Sierra Nevada block seismicity based on the double-difference method of Waldhauser & Ellsworth (2000).

A levelling profile along Highway 395, and trilateration measurements completed in 1980, showed that the resurgent dome in the central section of the caldera had developed a 25-cm domical uplift some time between the autumn of 1979 and the summer of 1980 (Savage & Clark 1982). Widespread earthquake activity at the $M3$

Fig. 2. Generalized geological map of the Long Valley Caldera–Mono Domes volcanic field, showing the principal volcanic units (after Bailey *et al.* 1976). Heavy black lines are major range-front faults. FLF, Fern Lake Fault; HCF, Hilton Creek Fault; HSF, Hartley Springs Fault; LVF, Lee Vining Fault; RVF, Round Valley Fault; and SLF, Silver Lake Fault. Small circles are $M>2$ earthquakes for 1978–2004. WC is Wheeler Crest.

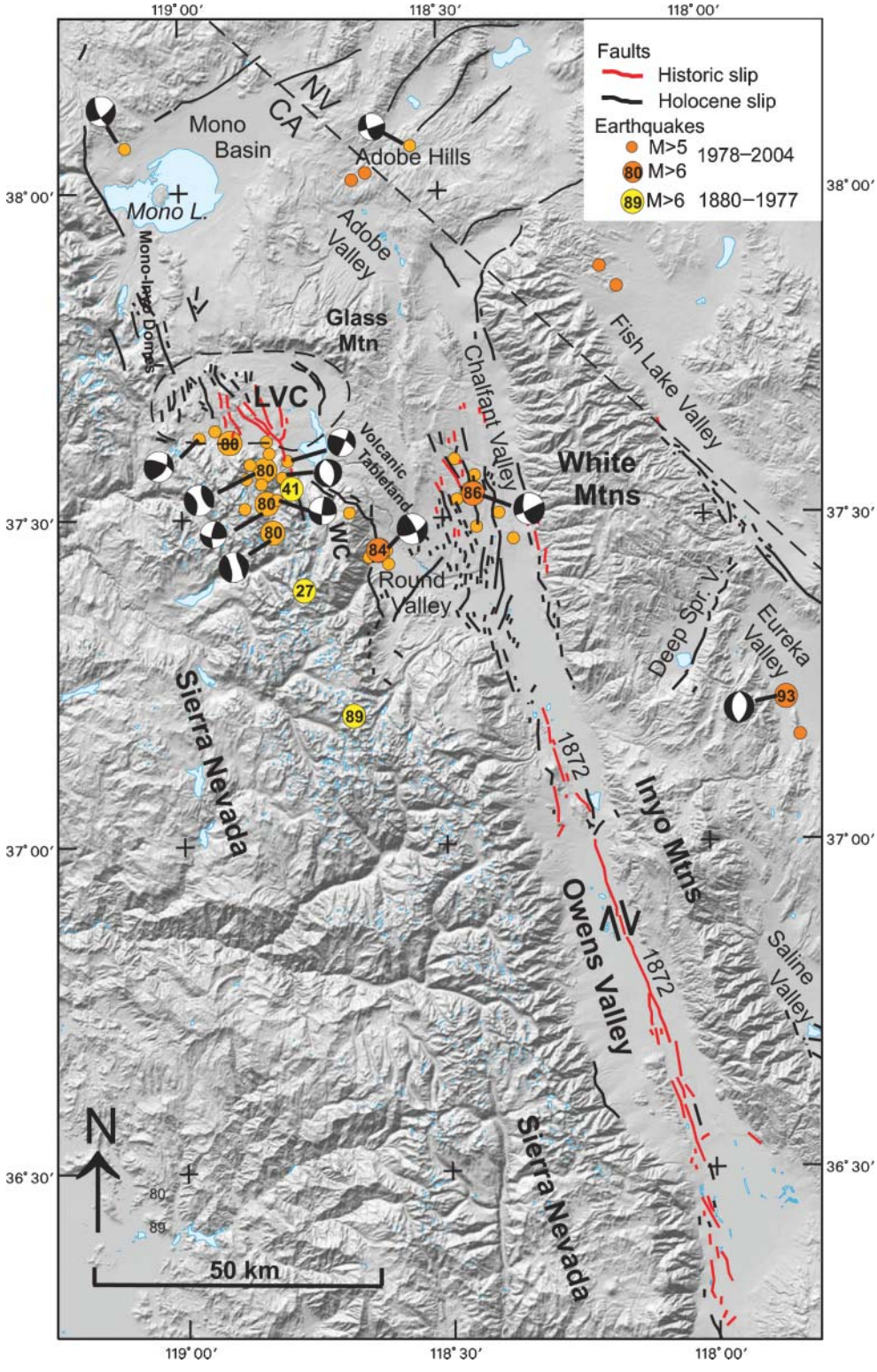
119° 00′
118° 30′
118° 00′
38° 00′
37° 30′
37° 00′
36° 30′
Faults
Historic slip
Holocene slip
Earthquakes
M>5 1978–2004
80 M>6
89 M>6 1880–1977
NV
CA
Mono Basin
Mono L.
Adobe Hills
Adobe Valley
Mono-Inyo Domes
Glass Mtn
LVC
Volcanic Tableland
WC
Chalfant Valley
Fish Lake Valley
White Mtns
Round Valley
Deep Spr. V.
Eureka Valley
Sierra Nevada
1872
Inyo Mtns
Owens Valley
Saline Valley
Sierra Nevada
80
41
86
84
27
89
93
N
50 km

to $M4$ level continued through the early 1980s in both the Sierra Nevada block south of the caldera and the SMSZ within the caldera. This activity included an $M=5.9$ event on 30 September 1981 that was located beneath the west end of the Convict Lake–Mount Morrison (CL–MM) cluster and just 2 to 3 km west of the initial $M=6.1$ earthquake of May 1980 and 2 to 3 km south of the caldera (Fig. 4b). Most of the aftershocks to this $M=5.9$ earthquake occurred within the caldera to the north, and were concentrated in the east lobe of the SMSZ and along the southeastern margin of the resurgent dome. By the summer of 1982, a locally dense seismic network and the beginnings of the current deformation-monitoring network had been installed (Fig. 6).

On 7 January 1983, an intense earthquake swarm, which included two $M=5.3$ earthquakes and a multitude of smaller events, began in the west lobe of the SMSZ and rapidly spread to the entire SMSZ. As documented by Savage & Cockerham (1984), this swarm was accompanied by an additional 7 cm uplift of the resurgent dome (Fig. 7) and by roughly 20 cm of right-lateral slip along the SMSZ. They found that the deformation field also admitted the possibility that the swarm was accompanied by a sheet-like intrusion of magma or a hydrous magmatic fluid to within 4 km of the surface beneath the south moat from a source beneath the resurgent dome. Occasional smaller swarms through the remainder of 1983 and the first half of 1984 followed the January 1983 swarm, which gradually subsided in intensity over the next several months (Fig. 5).

Slowing caldera unrest and regional earthquakes: 1984–1988

Following an $M=4.2$ earthquake beneath the south margin of the caldera on 28 April 1984 and an earthquake swarm that included $M=3.6$ and $M=3.2$ earthquakes in the west lobe of the SMSZ in the last half of July 1984, activity within the caldera declined to a relatively low level that persisted through early 1989 (Figs 5 & 7). Regional earthquake activity continued, however, with an $M=6.1$ earthquake in Round Valley 20 km southeast of the caldera on 23 November 1984 (Priestley *et al.* 1988) and an $M=6.4$ earthquake in Chalfant Valley, 30 km east of the caldera (Fig. 3) on 21 July 1986 (Smith & Priestley 1988). The Chalfant earthquake sequence was particularly intense. It was preceded by an energetic foreshock sequence that increased in intensity during the month prior to the $M=6.4$ mainshock, and included a $M=5.9$ earthquake 24 hours before the mainshock. The protracted aftershock sequence included four $M>5$ earthquakes, the largest of which was a $M=5.8$ event on 31 July.

Meanwhile, seismicity within the caldera remained low, and deformation measurements showed continued but slowing tumescence of the resurgent dome, with the uplift rate dropping below 1 cm per year from 1984 through late 1988 and showing slight subsidence in 1989 (Fig. 7). The cumulative uplift over the central part of the resurgent dome, with respect to its pre-1980 level, exceeded 40 cm by mid-1989 (Savage 1988; Langbein 1989).

The 1989 Mammoth Mountain swarm, long-period earthquakes and CO_2 emissions

In early May 1989, as the resurgent dome showed slight subsidence and the caldera remained quiet, an 11-month-long swarm of small earthquakes began under Mammoth Mountain on the southwest rim of the caldera (Figs 5 & 8b; the MM cluster in Fig. 4b) and persisted into early 1990. Although the swarm was not particularly energetic, it was prolonged. It was accompanied by minor deformation (1–2 cm of uplift), but included only three $M\approx 3$ earthquakes, in addition to thousands of smaller earthquakes and frequent spasmodic bursts (Langbein *et al.* 1993; Hill & Prejean 2005). High-resolution hypocentral locations for the swarm earthquakes obtained by (Prejean *et al.* 2003) define a dyke-like seismicity keel at depths of 7 to 10 km beneath the south flank of Mammoth Mountain, with a NNE strike, which is overlain by an ellipsoidal volume in the upper 6 km of the crust, defined by a series of seismicity rings centred about the summit at successively shallower depths (Fig. 9). The initial swarm activity began at the intersection of the lower seismicity ring with the keel at a depth of *c.* 6 km and propagated circumferentially around the ring and to shallower depths at rates of *c.* 0.4 to 1–2 km/month, respectively (Prejean *et al.* 2003). These

Fig. 3. (**a**) Shaded relief map illustrating the relation of Long Valley Caldera (LVC) to major tectonic elements and $M>5$ earthquakes in eastern California (the red rectangle in inset shows the map area). Heavy black and red lines are faults with Holocene slip and historic (post-1870) slip, respectively. The surface trace of the $M=7.8$ Owens Valley earthquake of 1872, labelled '1872'. Orange circles are post-1977 earthquakes (small for $M>5$; large with decadal year included for $M>6$). Yellow circles are 1870–1978 $M>6$ earthquakes (not including aftershocks to the 1872 mainshock) with decadal year indicated. WC is Wheeler Crest.

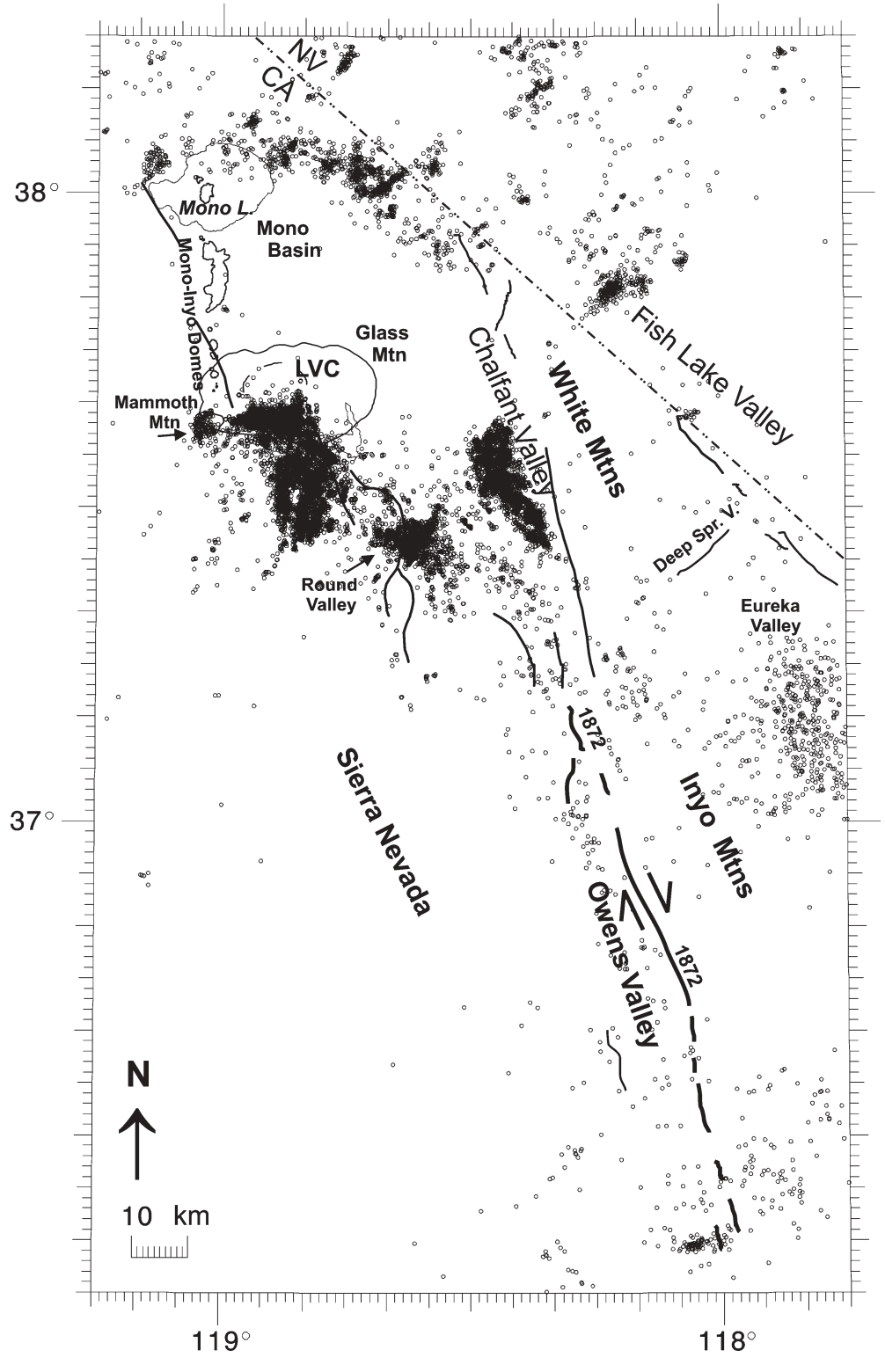
NV
CA
38°
Mono L.
Mono
Basin
Mono-Inyo Domes
Glass
Mtn
LVC
Mammoth
Mtn
Chalfant Valley
White Mtns
Fish Lake Valley
Deep Spr. V.
Round
Valley
Eureka
Valley
1872
Sierra Nevada
Inyo Mtns
Owens Valley
1872
37°
N
10 km
119°
118°

propagation rates are consistent with the seismicity being driven by a hydrous fluid flow through crystalline rocks with hydraulic diffusivities $D = 0.03$ to 0.2 m^2 s^{-1} (Hill & Prejean 2005).

The 1989 Mammoth Mountain swarm marked the onset of: (1) a continuing series of deep, long-period (LP) volcanic earthquakes centered at depths of 10 to 25 km beneath the southwest flank of Mammoth Mountain and the Devil's Postpile (DLPs in Fig. 4); (2) the diffuse emission of cold, magmatic CO_2 in the soil in several areas around the flanks of Mammoth Mountain; and (3) an elevated $^3He/^4He$ ratio (Sorey *et al.* 1993; Farrar *et al.* 1995). Both the deep LP earthquakes and CO_2 emissions have continued through mid-2005, and both appear to be related to the presence of basaltic magma distributed in a plexus of dykes and sills at mid-crustal depths (10 to 25 km) beneath the southwest flank of Mammoth Mountain and Devil's Postpile (Sorey *et al.* 1998; Hill & Prejean 2005). This 1989 swarm appears to have been driven by the release of a volume of CO_2-rich, hydrous fluids from the upper reaches of the mid-crustal plexus of basaltic dykes and sills that subsequently diffused upward into the brittle crust to depths as shallow as 3 km beneath the edifice of Mammoth Mountain and venting the volatile CO_2 phase at the surface.

Unrest returns to the caldera: 1990–1995

Beginning in late September 1989 (midway through the Mammoth Mountain swarm), measurements with the two-colour Electronic Distance Meter (EDM) showed that renewed extension across the resurgent dome had begun abruptly from slight subsidence to a rate of more than 7 cm per year, heralding a return of unrest within the caldera (Figs 5 & 7). Three months later (early January 1990), earthquake swarm activity resumed in the south moat (Langbein *et al.* 1993) as the extension rate began slowing. By late March 1990, the extension rate had slowed to 2 to 3 cm per year, a rate that persisted with only minor variations through 1995 (Fig. 7). Earthquake swarm activity resumed in early 1990 beginning in the western lobe of the SMSZ (Figs 5 & 8b). By the end of 1990, it involved the east and west lobes, as well as much of the southern section of the resurgent dome. The two strongest swarms during this 1990–1995 period occurred during 24–27 March 1991 and late

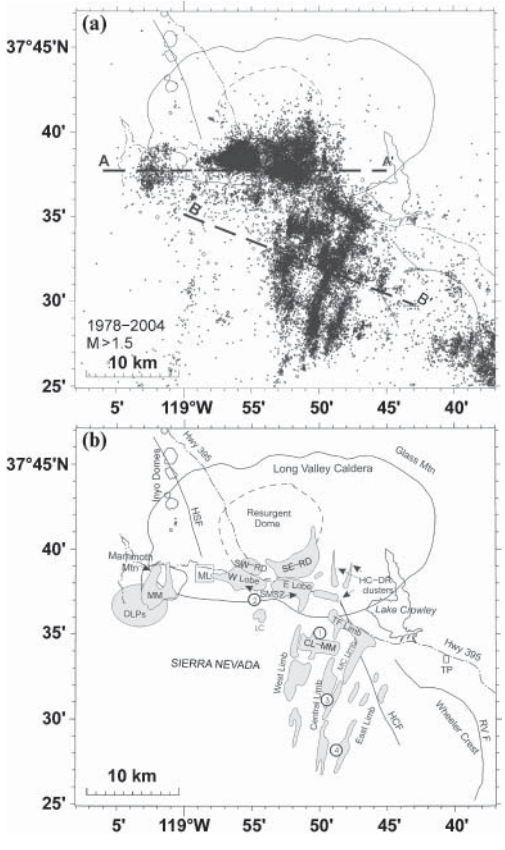

Fig. 4. (**a**) Seismicity patterns in Long Valley caldera and the adjacent Sierra Nevada block defined by $M \geq 1.5$ earthquakes for 1978–2004. Epicentres within the caldera are projected on to section A–A^1 and those in the Sierra Nevada block on to section B–B^1 for the space–time plots of Figure 5. Earthquake magnitudes are scaled by circle size from the smallest ($M = 1.5$) to the largest ($M = 6.2$). (**b**) Dominant seismicity clusters for the same period. Numbered circles are epicentres for the May 1980 $M > 6$ earthquakes numbered in order of occurrence (1–3 on 25 May, and 4 on 27 May). Abbreviations: CL–MM, Convict Lake–Mount Morrison; DLPs, deep long-period earthquakes (epicentres not plotted in (**a**); HC–DR, Hot Creek–Doe Ridge; LC, Laurel Creek; MC, McGee Creek; MM, Mammoth Mountain; SMSZ, south moat seismic zone with E (east) and W (west) lobes; SE–RD, southeast resurgent dome; SW–RD southwest resurgent dome; TF, Tobacco Flat. Heavy solid lines are major range-front faults: HCF, Hilton Creek Fault; HSF, Hartley Springs Fault; RVF Round Valley Fault. ML is Mammoth Lakes and TP is Tom's Place.

Fig. 3. (**b**) Epicentres for $M > 2$ earthquakes in same area as in (a) for 1978–2004.

November to early December 1993. Both were located in the west lobe of the SMSZ. The March 1991 swarm included more than 1000 detected earthquakes, with 22 $M > 3$ earthquakes, two of

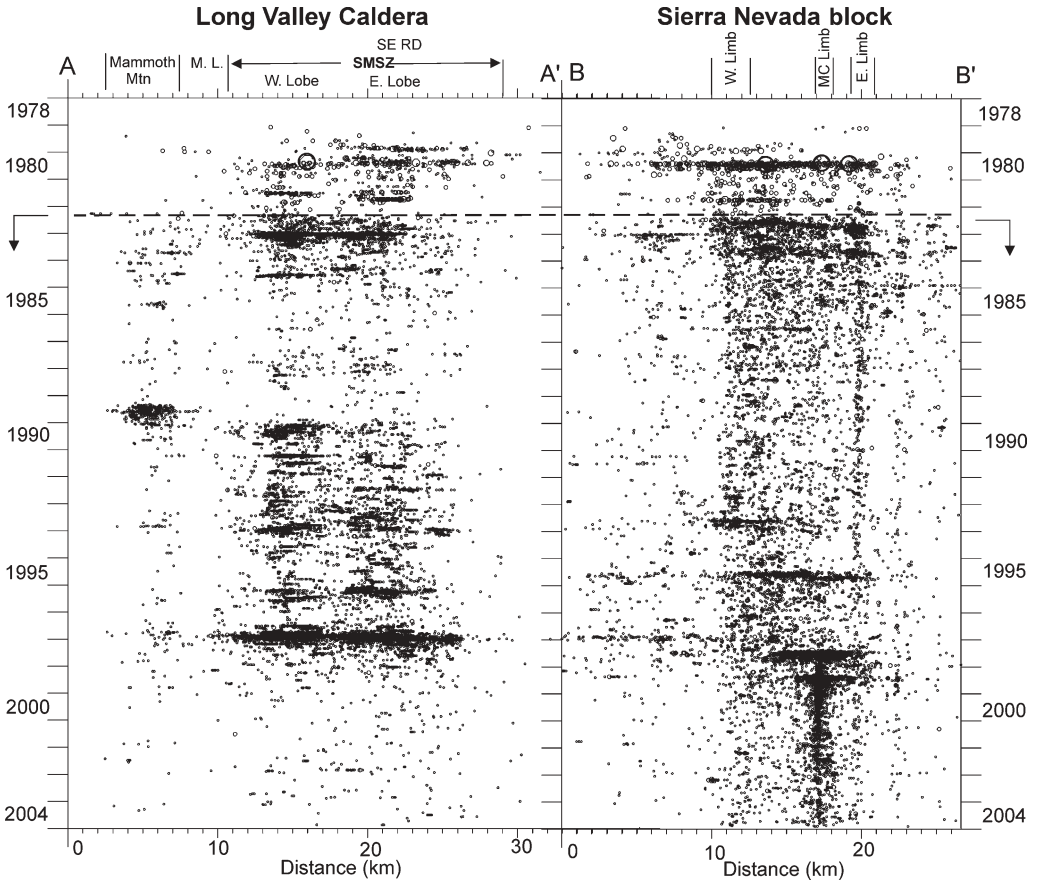

Fig. 5. Space–time plots with $M \geq 2$ earthquakes within the caldera projected on to profile A-A[1] and those within the Sierra Nevada block on to profile B-B[1] (Fig. 4a). Circle size scaled with magnitude from $M = 1.5$ to the largest circles for the four M 6 earthquakes of 25–27 May 1980. The dashed line in mid-1982 indicates when the locally dense, telemetered seismic network became operational with the capability of systematically locating all $M \geq 1.5$ earthquakes (prior to 1982, this completeness threshold was $M \approx 2.5$).

which had magnitudes of $M = 3.7$. The more energetic November–December 1993 swarm included $M = 4.0$ and 4.1 earthquakes.

A south-moat earthquake swarm on 28–30 June 1992, is particularly noteworthy – not because of its intensity but because of its timing. This swarm began *c*. 30 seconds after the S-wave from the $M = 7.3$ Landers earthquake of 28 June 1982, passed through the caldera. (The epicentre of the Landers earthquake was centred in the Mojave Desert some 400 km south of the caldera.) As it turned out, many areas across the western United States showed an abrupt increase in local seismicity rates following the Landers earthquake, providing the first clearly documented case of remotely triggered seismicity by a large, distant earthquake. At Long Valley Caldera, the strong surface waves from the Landers earthquake also triggered a transient, caldera-wide uplift that reached a peak strain of 0.3×10^{-6} (corresponding to a peak uplift of *c*. 5 mm) five to six days after the Landers earthquake. The June 1992 swarm itself included more than 250 located earthquakes distributed throughout the SMSZ, the largest of which was a $M = 3.4$ earthquake in the west lobe. Triggered seismic activity in the Sierra Nevada block immediately south of the caldera included a $M = 3.7$ earthquake (see Hill *et al.* 2002*b*).

Caldera earthquake activity and resurgent dome tumescence gradually slowed from early 1994 through early 1996 (Fig. 7). Earthquake activity in the Sierra Nevada block south of the caldera, however, continued at a relatively steady rate (Fig. 8c). Most of this 1990–1995 Sierra Nevada activity was concentrated in elongated

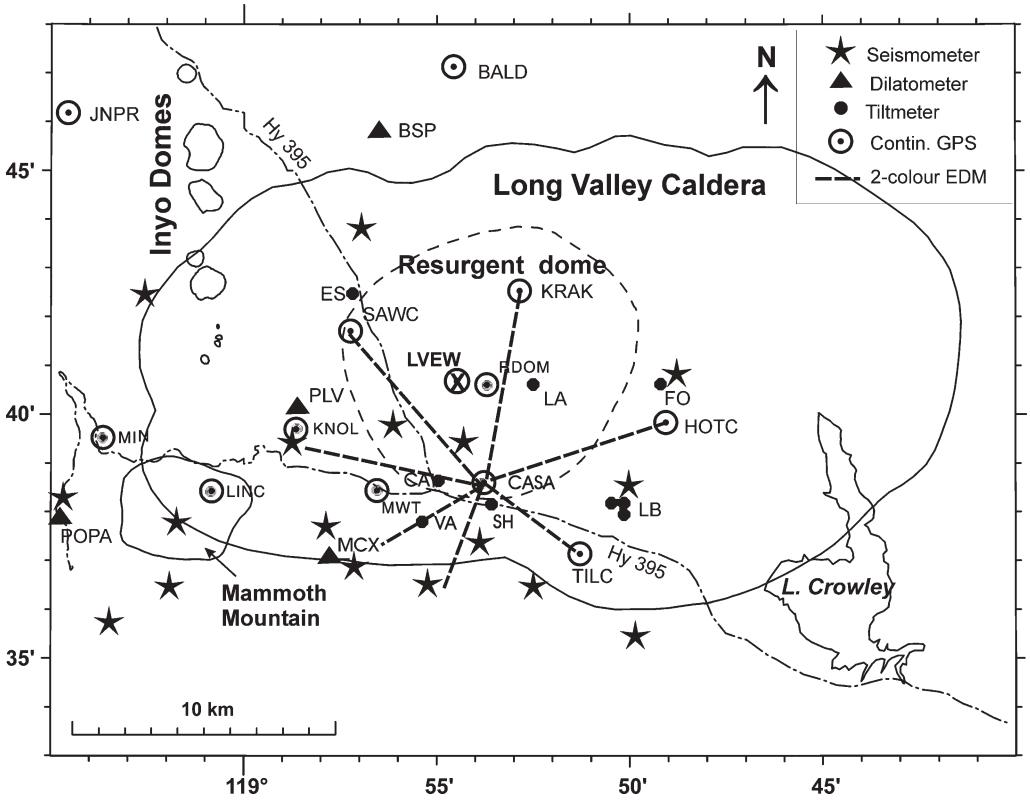

Fig. 6. Map showing instrument sites for seismic and deformation monitoring networks established beginning in the spring of 1982 (see Appendix D in Hill *et al.* 2002*a*). The heavy dashed line is the Casa-Krak 2-colour EDM (electronic distance meter) baseline. Length changes in this baseline closely track elevation changes at the centre of the resurgent dome (Fig. 7).

clusters forming the western, central, and eastern limbs of the NNE-trending seismicity lineations south of the caldera (Fig. 4), with the east-dipping, western limb producing most of the earthquakes. Particularly energetic sequences included a swarm on 10–15 August 1993 centred in the southern cluster of the west limb (Fig. 4b) and a series of swarms in the same general area that began in late June 1995 and persisted through late September. The August 1993 swarm included more than 400 $M > 1$ earthquakes, the largest of which had a magnitude of $M = 4.5$. The June–September 1995 swarms included over 20 $M > 3$ earthquakes, the largest of which was an $M = 3.7$ earthquake on 17 September.

The March–April 1996 south-moat earthquake swarm

In contrast to the general tendency of caldera earthquake-swarm activity to follow the uplift rate of the resurgent dome (Fig. 7), one of the strongest earthquake swarms in the caldera occurred in March and April of 1996 as inflation of the resurgent dome was slowing (Hill *et al.* 2003). This seismic sequence began as a series of small earthquake swarms in the east lobe of the SMSZ in early 1996 (Figs 4b & 8d). Activity gradually escalated in intensity through February and early March, culminating in late March and early April with what at the time was the most energetic earthquake swarm within the caldera since the January 1983 swarm. This activity included more than 24 earthquakes of $M = 3.0$ or greater, all located within the east lobe of the SMSZ. The three largest earthquakes included a pair of $M = 4.0$ events on 30 March and a $M = 4.3$ event on 1 April. Altogether, this swarm included more than 1600 earthquakes located by a real-time computer system ($M > 0.5$), and it had a cumulative seismic moment of roughly 5×10^{15} N m, or the equivalent of a single $M = 4.8$ earthquake.

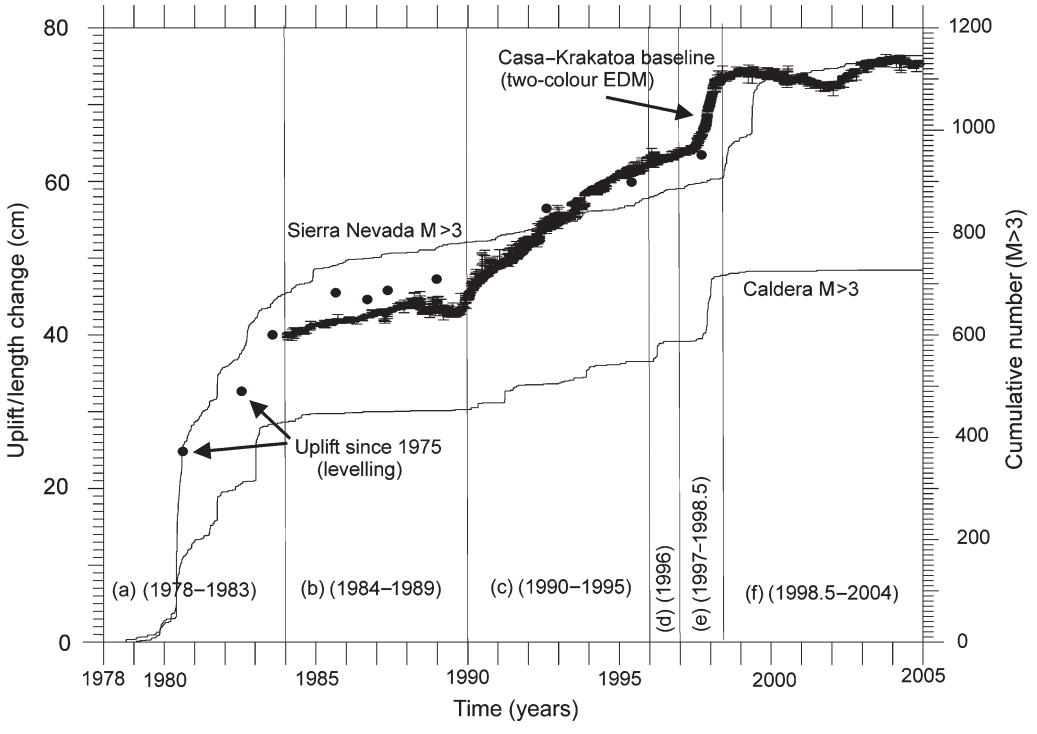

Fig. 7. Temporal variations in the cumulative number of $M \geq 3$ earthquakes in Long Valley caldera and the Sierra Nevada block for 1978–2004, together with the uplift history for the centre of the resurgent dome based on levelling surveys (solid circles) and extension of the Casa–Krakatoa EDM baseline (heavy black line – see Fig. 6 for baseline location). Time intervals (**a**) to (**f**) correspond to interval seismicity maps in Figure 8. The earthquake catalogues for this area are complete for $M \geq 3$ earthquakes throughout the 1978–2004 interval.

The deformation-monitoring networks showed no significant ground deformation associated with this 1996 earthquake swarm, suggesting that the swarm reflects relaxation of accumulated stress rather than the intrusion of a fluid volume into the brittle crust (Hill *et al.* 2003). Indeed, deformation of the resurgent dome continued to slow through 1996 and well into the spring of 1997 (Fig. 7). Subsequent seismic activity within the caldera included only three minor swarms in the west lobe of the SMSZ in June 1996, followed by nearly ten months of relative quiescence.

Strong caldera unrest: 1997 to mid-1998

By the end of April 1997, declining extension rates across the resurgent dome had dropped to less than 1 cm per year, while seismicity levels within the caldera remained low (Figs 5 & 7). Seismic activity outside the caldera during the first six months of 1997 included $M = 4.2$ and $M = 4.1$ earthquakes on 10 and 24 February, respectively – both located in the Sierra Nevada 4 km south of the caldera and 2 km south of Convict Lake (in the CL–MM cluster, Figs 4b & 8e). At roughly the same time, the rate of mid-crustal LP earthquakes beneath Mammoth Mountain increased markedly to an average of *c*. 20 events/week, sustained through much of 1997 and gradually slowing to a background rate fluctuating between two and five events/week through 2002 (Hill & Prejean 2005).

Then, after nearly a year of relative quiescence within the caldera, unrest gradually increased in mid-1997. The onset of renewed unrest first appeared in the two-colour EDM deformation data – as gradually accelerating extension across the resurgent dome in May and June, followed by the onset of minor earthquake-swarm activity in the west lobe of the SMSZ in early July (Figs 4b & 8e). The rates of resurgent dome tumescence and earthquake-swarm activity (both event rate and seismic moment rate) continued to increase through the summer and autumn, with peak rates of 0.2 cm/day and 1000 $M > 1.2$ events/day, respectively, on 22 November, and an average extension rate of 0.1 cm/day from

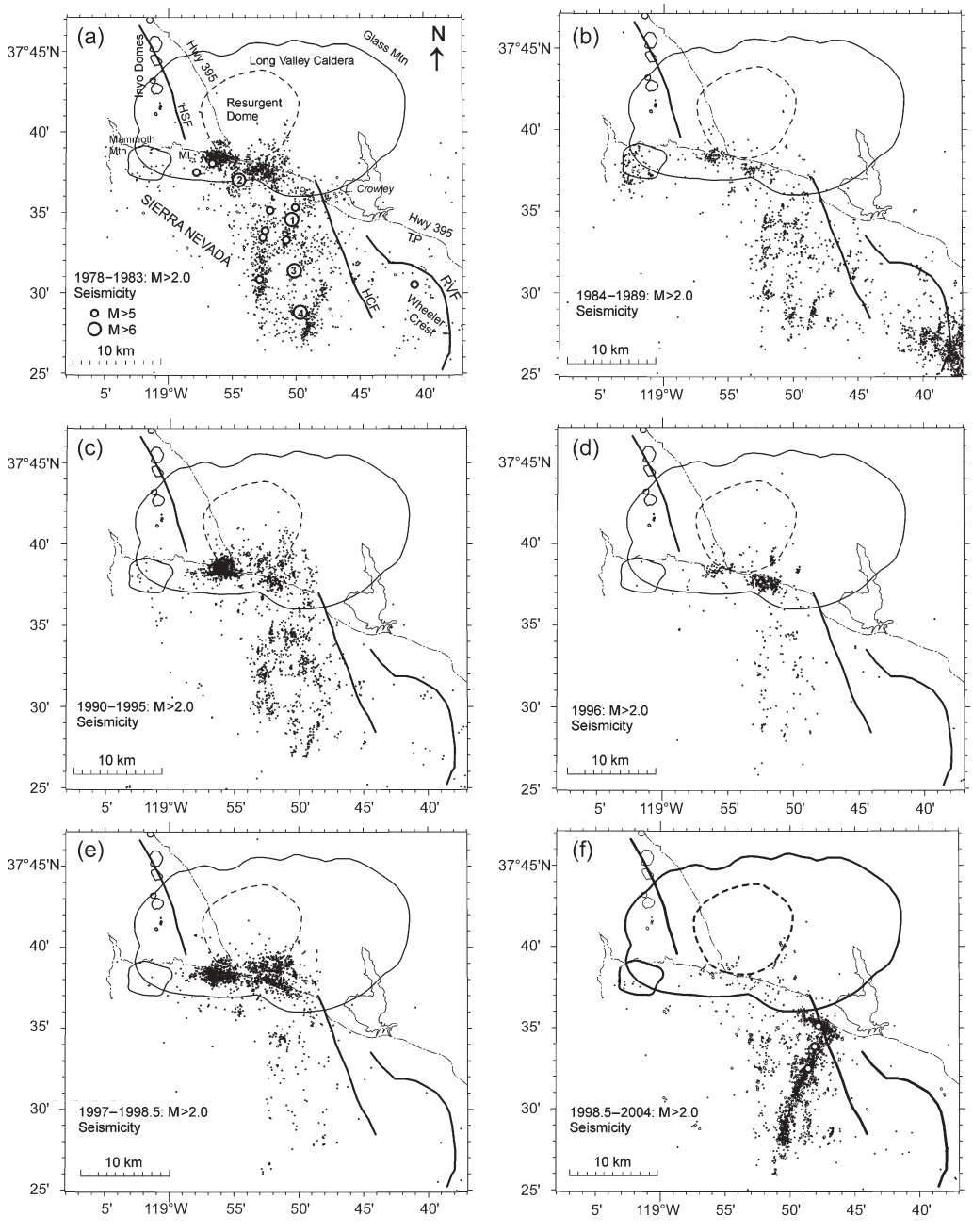

Fig. 8. Seismicity patterns for $M \geq 2$ earthquakes for the six time intervals (**a**) through (**f**) identified in Figure 7. Abbreviations as in Figure 4b.

mid-November to early December (Fig. 7). The earthquake-swarm activity was concentrated at depths between 3 and 8 km beneath a broad, 15-km-long zone spanning the entire SMSZ and the southern margin of the resurgent dome. It included more than 12 000 $M > 1.2$, 120 $M > 3.0$, and 8 $M > 4.0$ earthquakes during the seven-month period through mid-January, with a cumulative seismic moment of 3.3×10^{17} N-m (the equivalent of a single $M = 5.4$ earthquake).

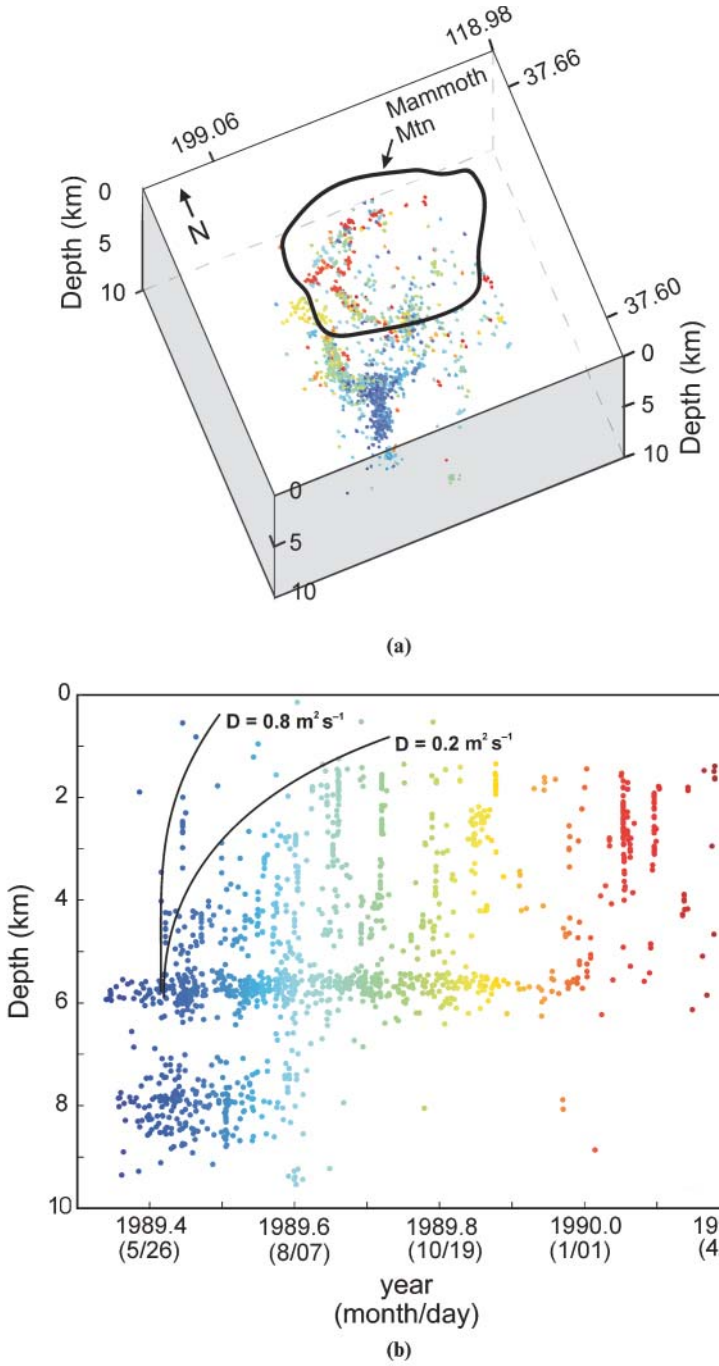

Fig 9. Space–time patterns of the 1989 Mammoth Mountain earthquake swarm, based on the double-difference hypocentral locations of Prejean *et al.* (2003). Figure adopted from Hill & Prejean (2005). (**a**) Three-dimensional perspective looking down to the NNE (N 23° E at an inclination of 76°). The black curve outlines the base of Mammoth Mountain (see Fig. 2). Hypocentre colours keyed to increasing time from purple to red. (**b**) Depth–time plot of 1989 swarm hypocentres with time color key. The curves labelled $D = 0.2$ m^2 s^{-1} and $D = 0.8$ m^2 s^{-1} show the range of hydraulic diffusivities, D, consistent with the vertical migration of the seismicity front being driven by the upward diffusion of a pore-pressure increase following the method of Shapiro *et al.* (1999). The horizontal propagation rates and diffusivities are an order of magnitude lower (see Hill & Prejean 2005).

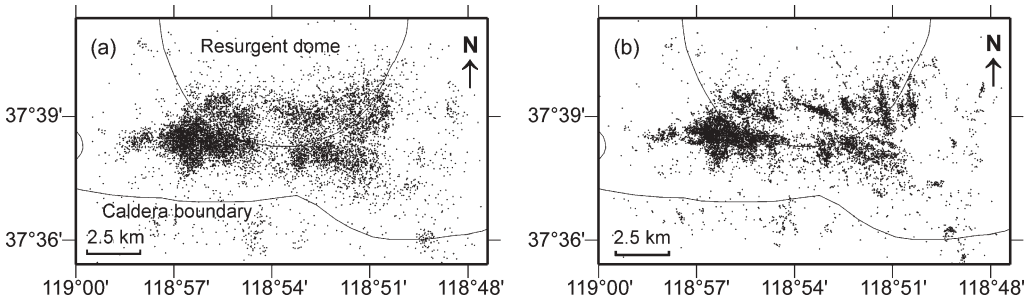

Fig. 10. Comparison of epicentral patterns for earthquakes in the SMSZ for the period July 1997 to January 1998, based on (**a**) the Northern California Earthquake Data Center (NCEDC) archive catalogue locations, and (**b**) the high-resolution locations obtained using the double-difference relocation algorithm of Waldhauser & Ellsworth (2000). Adapted from Prejean *et al.* (2002) with permission.

The 1997 seismic-moment release was dominated by right-lateral slip along the WNW-trending fault zone beneath the south moat. The great majority of swarm earthquakes had the broad-band character of brittle, double-couple events (tectonic or 'volcano-tectonic' earthquakes). An important subset, however, had energy concentrated in the 1- to 3-Hz band typical of LP volcanic earthquakes, as well as non-double-couple focal mechanisms with a significant isotropic (opening) component consistent with fluid intrusion and a local volume increase (Dreger *et al.* 2000; Foulger *et al.* 2004; Prejean *et al.* 2002). Both the earthquake-swarm activity and inflation of the resurgent dome declined to background levels through March. By the end of March, inflation of the resurgent dome had essentially stopped, at which point the centre of the resurgent dome stood roughly 10 cm higher than in the spring of 1997 (and 75–80 cm higher than the pre-1980 profile; see Fig. 7). The 1997 to mid-1998 earthquake activity was exceeded in intensity only by the January 1983 swarm with two $M = 5.3$ earthquakes and the May 1980 sequence with two of four $M \approx 6$ earthquakes within or immediately adjacent to the caldera.

Precise relocations of the 1997 south-moat swarm earthquakes obtained by Prejean *et al.* (2002) resolve the diffuse cloud of epicentres evident in Fig. 8e into a series of narrow, subparallel, WNW-striking seismicity lineations that represent individual faults beneath the south moat activated during the swarm (Fig. 10). The lineations along the northern margin of the swarm distribution have a distinct northerly dip, such that the associated fault planes are inclined beneath the resurgent dome in the general direction of the inflation source driving uplift of the resurgent dome at a depth of 6 to 8 km. The precise hypocentral locations for the peak surge in swarm activity on 22 November reveal that the activity began near the base of the seismogenic crust at a depth of *c.* 8 km on one of the north-dipping faults, and then propagated both to the west and to shallower depths at a rate of *c.* 0.5 km/h. Prejean *et al.* (2002) find that this same pattern applies to earlier swarm sequences in the west lobe of the SMSZ, but with the seismicity-fronts propagating at considerably lower rates (e.g. *c.* 0.002 km/h, and *c.* 0.008 km/h for swarms in November 1993 and July 1984, respectively). These results, together with the positive isotropic component associated with the non-double-couple moment tensors, suggest that south-moat swarm activity is driven by the injection of high-pressure hydrous magmatic fluids into the brittle crust from the subjacent magma body responsible for inflation of the resurgent dome (Prejean *et al.* 2002). Variations in seismicity-front propagation rates likely depend on variations in transient fracture permeability, which may vary from one swarm to the next.

Mammoth Mountain, which had been relatively quiet since the 1989 earthquake swarm, joined the elevated caldera activity in early September 1997, with the onset of a swarm of brittle-failure earthquakes in the upper 10 km of the crust that played out through December. This swarm included a $M = 3.2$ earthquake on 1 October, located at a depth of 3.4 km beneath the north flank of Mammoth Mountain. The swarm coincided with a marked increase in CO_2 soil-gas concentrations around the flanks of the mountain, an increase that persisted from September to December (McGee *et al.* 2000). This is the only instance in which Mammoth Mountain swarm activity has coincided with elevated activity within the caldera.

Caldera quiescence and M > 5 *earthquakes in the Sierra Nevada block: mid-1998 to 1999*

By mid-spring of 1998, unrest within the caldera had declined to negligible levels (Figs 5 & 7). Deformation data showed that swelling of the resurgent dome had essentially stopped and seismic activity within the caldera involved just a few small ($M < 3$) earthquakes per day. The caldera has remained quiet, with virtually no additional deformation through mid-2005. Meanwhile, the focus of seismic activity shifted to the Sierra Nevada block south of the caldera, with $M = 5.1$ earthquakes on 8 June and 14 July 1998, and a $M = 5.6$ earthquake on 15 May 1999 (Figs 5, 7 & 8f).

All three $M \geq 5.1$ earthquakes occurred within the footwall block of the east-dipping Hilton Creek Fault with epicentres located 1.5, 4.2 and 8.0 km south of the caldera boundary, respectively (Fig. 8f). The rich aftershock sequences to these $M \geq 5.1$ earthquakes define an orthogonal pattern with the apex pointing eastward toward Lake Crowley (the TF and MC limbs in Figs 4b & 8f) and the SSW MC (McGee Creek) limb extending some 14 km into the Sierra Nevada south of the caldera at an acute angle to the central limb defined by earlier activity. The southeast trend of aftershocks to the 8 June mainshock coincides with the right-lateral slip plane of the strike-slip focal mechanism for this event, and the SSW trend defined by the aftershocks to the 14 July 1998, and 15 May 1999, events coincides with the left-lateral plane of the dominantly strike-slip focal mechanism for the $M = 5.6$ event of 15 May. The focal mechanism for the 14 July mainshock was dominantly normal, with a northerly strike (Prejean *et al.* 2002). All three focal mechanisms have the direction of maximum extension (T-axes) oriented to the ENE.

Although aftershocks to the three $M > 5$ earthquakes south of the caldera have gradually waned, the aftershock zone has continued to dominate seismic activity in the Sierra Nevada block since 1999. Long Valley Caldera itself had remained relatively quiet since mid-l998, with virtually no seismicity at the $M > 3$ level, and only minor fluctuations in the elevation of the resurgent dome through late 2004 (Figs 5 & 7).

Aside from a few brief earthquake swarms, occasional mid-crustal LP earthquakes, and sustained CO_2 outgassing at a rate of *c*. 300 tonnes/day, Mammoth Mountain has remained largely quiet since the 1997 activity. Two additional Mammoth Mountain phenomena, however, deserve special note. One involves the occurrence of three very-long-period (VLP) volcanic earthquakes at shallow depths (*c*. 3 km) beneath the summit – one in October 1996 and one each in July and August 2000, respectively (Hill & Prejean 2005). These LVP earthquakes, which were accompanied by local spasmodic bursts and LP earthquakes, apparently resulted from a slug of a CO_2-rich, hydrous fluid moving through a crack-like restriction. Because spasmodic bursts were common during the 1989 swarm, it seems likely that VLP earthquakes may have occurred then as well, although we had no means of detecting them at the time (Hill & Prejean 2005).

The other phenomena involve two minor earthquake sequences triggered by large, distant earthquakes. Brief flurries of small ($M < 2.3$) earthquakes occurred beneath the north flank of Mammoth Mountain, immediately following the $M = 7.2$ Hector Mine earthquake of 16 October 1999 (epicentral distance *c*. 420 km) and beneath the south flank as the surface waves from the $M = 7.9$ Denali Fault earthquake of 3 November 2002 (epicentral distance *c*. 3 460 km) propagated through the area. In both cases, local strain transients recorded on nearby borehole strainmeters were significantly larger than can be explained by the cumulative seismic slip for the swarm earthquakes, implying the dominant triggered response was aseismic slip and/or fluid intrusion (Johnston *et al.* 2004; Prejean *et al.* 2004). Both of these phenomena point to the active transport of hydrous fluids in the crust beneath the mountain (Hill & Prejean 2005).

Discussion: sources of caldera unrest and tectonic–magmatic interactions

The decades-long correlation between episodic unrest within Long Valley Caldera and elevated seismic activity in the surrounding region emphasizes that tectonic–magmatic interactions are key to understanding the processes driving caldera unrest and, more generally, volcanism in the eastern Sierra Nevada. Seismic activity levels at the $M > 3$ level within the caldera and the Sierra Nevada block to the south in particular are closely correlated with each other and with deformation within the caldera when averaged over two or more years (Fig. 7). The occurrence of the $M \approx 6$ Round Valley earthquake in November 1984, the $M \approx 6.4$ Chalfant Valley earthquake in July 1986, and the $M = 6.1$ Eureka Valley earthquake of May 1993, suggests a more

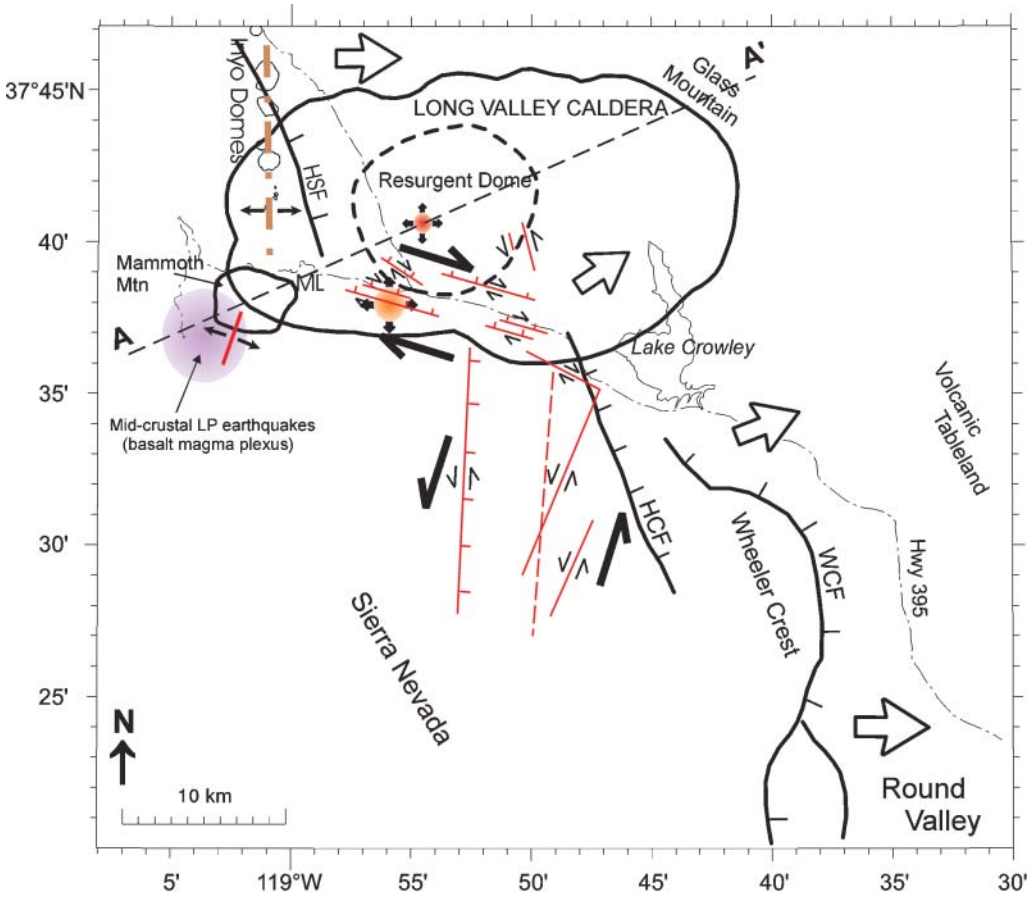

Fig. 11. A schematic representation of basic kinematic relations between dominant seismogenic and magmatic sources contributing to unrest within the caldera and the Sierra Nevada block to the south for the period 1978–2004. Profile A–A[1] indicates orientation of the cross-section in Figure 12. Thin red lines are inferred faults based on the high-resolution hypocentral locations and focal mechanisms of Prejean *et al.* (2002). The dashed red lines are lineations defined by the 1982–1995 seismicity (Fig. 7 (a) to (c)). Opposing half-arrows indicate relative sense of strike-slip displacement. Hash marks are in a down-dip direction on faults with dip-slip displacement components. (Note that the inferred faults depicted in Figure 9 have no clear surface expression as is common for faults associated with $M \approx 6$ or smaller earthquakes.) Orange circles with radial arrows indicate inflation centres with the resurgent dome inflation source centred at a depth z of c. 6–7 km and the SMSZ inflation source somewhere in the depth range z of c. 10–15 km. The purple pattern overlies the volume of mid-crustal LP earthquakes and the inferred plexus of basaltic dykes and sills. A thick red line beneath Mammoth Mountain indicates the seismicity keel ($z = 7$–10 km) that developed during the 1989 swarm, with arrows indicating the T-axis (extension direction). The thick brown dash–dot line indicates the position of the silicic dyke that fed the c. 650-ka Inyo Domes eruptions. Large open arrows indicate regional variation in the extension direction with respect to a fixed Sierra Nevada block based on the stress inversion of Prejean *et al.* (2002).

regional interaction as well. In this discussion, however, we focus on the more compelling interactions between unrest in the magmatic systems underlying the caldera and Mammoth Mountain and the seismic activity in the adjacent Sierra Nevada block, as illustrated schematically in Figures 11 & 12.

Seismogenic sources

The dominant seismogenic sources from 1978 to 2004 form a conjugate set of WNW-striking dextral faults within the SMSZ and the caldera, and NNE-striking sinistral faults forming a 10-km-wide zone within the Sierra Nevada

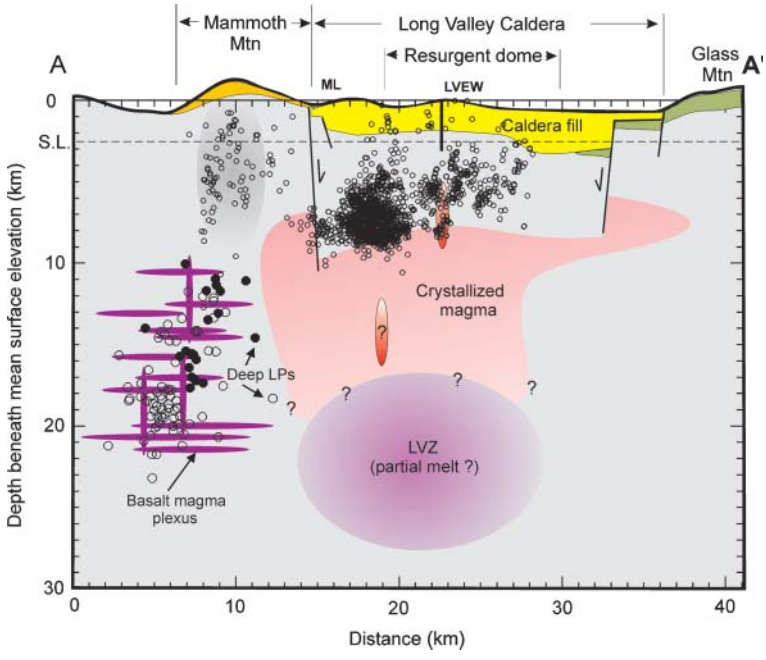

Fig. 12. Schematic cross-section A–A[1] through Long Valley Caldera (see Fig. 9) illustrating depth relations between the structural and magmatic elements contributing to caldera unrest. Geological units adopted from Bailey (2004). LVEW is the 3-km-deep well in the centre of the resurgent dome. Small circles are hypocentres for $M \geq 2$ earthquakes within the caldera and beneath Mammoth Mountain for 1978–2004 within 5 km of the cross-section. Large circles are mid-crustal LP earthquakes. Filled circles indicate LP events with hypocentres constrained by a dense, temporary seismic network deployed in 1997 (Foulger *et al.* 1998). Orange ellipsoids indicate inflation sources inferred from deformation data (Langbein 2003). The source centred 6–7 km beneath the resurgent dome is behind (north of) the SMSZ seismicity, which shallows to less than 6 km beneath the resurgent dome. The structure in the upper *c*. 10 km is generally well resolved by multiple seismological, geophysical and geological studies. Deeper structure (>10 km) is less certain, but includes evidence from teleseismic tomographic studies for a volume of low P-wave velocities (LVZ) in the 15–30-km depth range (e.g. Dawson *et al.* 1990; Weiland *et al.* 1995).

block south of the caldera (Fig. 11). Cramer & Toppazada (1980) recognized that this geometry is consistent with local ENE extension, such that the crustal block, including the caldera north of the SMSZ, is moving to the ENE with respect to the corner of the Sierra Nevada south and west of the caldera. Kinematically, this geometry requires an opening (extensional) mode within one or both of these fault zones. In principle, then, these are 'leaky' strike-slip fault zones providing potential pathways for magmatic fluids to migrate into the upper 10 km of the crust from mid- to lower-crustal depths. Indeed, focal mechanisms for a subset of earthquakes in both fault zones involve significant oblique–normal displacement components consistent with local extension (Prejean *et al.* 2002). The SMSZ in particular shows symptoms of a leaky strike-slip fault, with: (1) earthquake-swarm sequences propagating upward and outward from initiation nuclei at the base of the seismogenic crust; (2) numerous earthquakes with emergent, low-frequency onsets and significant isotropic components consistent with a local volume increase (Dreger *et al.* 2000; Foulger *et al.* 2004; Prejean 2002); and (3) co-seismic water-level and deformation transients that are significantly larger than can be explained by cumulative seismic slip for the associated earthquakes (Roeloffs *et al.* 2003). Furthermore, the SMSZ forms an oblique angle to the NNE strike of both the Hilton Creek and Hartly Springs range-front normal faults (Fig. 11). Kinematically, this corresponds to transtensional opening, to the extent that the SMSZ represents a dextral transform fault linking the left-stepping offset between normal faults (note that a strike-slip 'transform' fault forming right angles with offset normal faults does not include an opening displacement component).

Whether the NNE-striking sinistral fault system in the Sierra Nevada south of the caldera might be 'leaky' is not clear. Hough *et al.* (2000) see evidence in seismograms that some of the aftershocks to the 14 July 1998 $M = 5.2$ earthquake in the Sierra Nevada had a significant low-frequency component similar to LP volcanic earthquakes. Seismic activity occurs in both mainshock–aftershock and swarm-like sequences. Current deformation networks and geochemical and hydrological monitoring networks, however, do not extend into the rugged topography of the Sierra Nevada.

Of particular note is the fact that the Hilton Creek Fault and the other large, range-front normal faults defining the eastern escarpment of the Sierra Nevada (solid lines in Fig. 11) have not participated in the 1978–1999 activity in any significant way. Nevertheless, the overall extension direction associated with the recent earthquake activity is essentially perpendicular to the NNW strike of these large, range-front, normal faults, and thus consistent with the geological evidence for pure dip-slip displacement on these faults in Holocene times (Fig. 11). Prejean *et al.* (2002) find in their stress inversion of focal mechanism data that stresses within the caldera are currently dominated by the regional field, with the least principal stress direction rotating systematically in a clockwise direction from a NE–SW orientation within the caldera and the SMSZ to a more easterly orientation in the vicinity of Round Valley south of the caldera (see Fig. 11). This raises important questions regarding temporal variation in slip partitioning between (1) major ($M \approx 7$) dip-slip earthquakes on range-front faults; (2) the intervening moderate seismicity ($M \leq 6$) strike-slip earthquake in the footwall block of the sort that has dominated the 1978–2004 interval; and (3) extension (dyke intrusion) across the Inyo–Mono chain. An obviously related question is what influence do major range-front-fault earthquakes have on the Long Valley Caldera–Mono Domes magmatic system? Bursik *et al.* (2003), for example, cite evidence that the *c.* 1350 AD eruptions of the Inyo Domes may have coincided with a cascading sequence of earthquakes on adjacent sections of the Hartley Springs Fault.

Magmatic sources

The dominant magmatic sources contributing to the 1978–2004 unrest identified in Figures 11 and 12 include: (1) a compact inflation source centred 6 to 7 km beneath the central section of the resurgent dome; (2) a secondary inflation source centred somewhere beneath the western lobe of the SMSZ within the caldera, and (3) a plexus of basaltic dykes and sills coincident with the mid-crustal LP volcanic earthquakes at depths of 10 to 25 km beneath the southwest flank of Mammoth Mountain.

Deformation within the caldera is dominated by the symmetrical inflation of the resurgent dome. Langbein (2003) finds that most (>90%) of the deformation field within the caldera can be explained in terms of a spatially compact inflation source in the form of a near-vertical, pipe-like, prolate ellipsoid in the depth range 5 to 8 km centred beneath the resurgent dome together with dextral slip distributed across the SMSZ. Newman *et al.* (2006) show that modelling the compact prolate ellipsoid inflation source as encased in a viscoelastic shell serves to increase the effective source volume, thus reducing the pressure increase required to produce the observed uplift. Battaglia & Vasco (2006, this volume, pp. 173–180**)** find that the deformation data can be equally well fitted by a spatially distributed inflation source in the same 5- to 8-km depth interval underlying much of the southern half of the resurgent dome with a lobe extending toward the north rim of the caldera beyond the resurgent dome. They do not argue, however, that the distributed source represents a more realistic physical model – only that it illustrates the degree of non-uniqueness in modelling deformation data. In any case, resurgent dome deformation is typically much larger than can be accounted for by the associated swarm earthquakes within and immediately adjacent to the caldera. Furthermore, the onset of accelerated deformation generally precedes increases in earthquake activity by several weeks (Hill *et al.* 2003; Langbein *et al.* 1993). Both suggest that earthquake activity within the caldera is a symptom of (and secondary to) a more fundamental process associated with inflation of the resurgent dome.

The SMSZ seismicity appears not to be directly driven by stresses associated with resurgent dome inflation, however. Neither the spatial distribution of earthquakes within the caldera nor their focal mechanisms reflect the circular symmetry of resurgent-dome inflation evident in the geodetic data (Langbein 2003) and InSAR images (Thatcher & Massonnet 1997; Newman *et al.* 2006). Indeed, Prejean *et al.* (2002) conclude that stress associated with inflation of the resurgent dome produces only a minor perturbation on the regional stress field within the caldera. Rather, it appears as though SMSZ seismicity is modulated by episodic invasion of high-pressure

hydrous fluids into the brittle crust from the vicinity of the inflation source beneath the resurgent dome, under a stress field dominated by more regional processes (Prejean *et al.* 2002; Prejean 2002).

A standing question with regard to deformation in restless calderas centres on whether tumescence results from the addition of new magma into an upper-crustal magma body or a pressure increase associated with the exsolution of magmatic volatiles in a cooling (crystallizing) magma body or the heating of geothermal fluids. The latter has been proposed as an explanation for calderas with alternating periods of inflation and subsidence in the last three decades with no intervening eruptions such, as Yellowstone (United States) and Campi Flegrei (Italy) (see De Natale *et al.* 1991; Battaglia *et al.* 2003). This model appeals to increasing pressure in the upper reaches of a crystallizing magma body as the volatile phases accumulate beneath a low-permeability seal (a volume increase with no added mass). The onset of caldera subsidence results when low-permeability seals rupture, allowing depressurization and ground subsidence as the accumulated volatiles diffuse away into the overlying brittle crust (Fournier 1999).

Deformation in Long Valley Caldera, however, has yet to show significant subsidence (Fig. 7). Rather, caldera deformation has evolved as episodic uplift at varying rates through 1999, with only minor fluctuations during the four years of relative caldera quiescence from 2000 to mid-2005. As of mid-2005, the centre of the resurgent dome remains *c*. 75 cm higher than in the late 1970s, in spite of nearly four years of quiescence within the caldera (Figs 5 & 7). This, together with evidence from: (1) space–time seismicity patterns, focal mechanisms and transient deformation patterns, indicate that periods of accelerated inflation result from the injection of hydrous fluids into the brittle crust from the subjacent magma body (Roeloffs *et al.* 2003; Prejean 2002); and (2) results from repeated micro-gravity measurements indicating a mass increase beneath the resurgent dome with a density in the range 1180 to 2330 kg m^{-3} (Battaglia *et al.* 2003), suggests that the Long Valley caldera resurgent-dome tumescence is driven by the addition of mass in the 6- to 7-km-deep inflation source. Battaglia *et al.* (2003) suggest that, on the basis of the relatively low density, this mass may be a combination of magma and a gas-rich hydrous fluid.

The size, geometry and longevity of a magma body beneath the resurgent dome, however, remain important research targets. The resolution of published seismic tomography studies is still not adequate to distinguish clearly between conflicting models for the seismic velocity structure in the upper 15 km of the crust. Results based on studies using local earthquake sources appear to preclude significant low-velocity volumes in the upper 10 to 15 km of the crust (Kissling 1988; Tryggvason *et al.* 1998), while models based on S-wave attenuation tomography and teleseismic tomography indicate that volumes with relatively high S-wave attenuation and or low P-wave velocities (as low as 4.8 to 5.1 km s^{-1}) and lateral dimensions of 5 to 10 km underlie either the west moat, the south moat or the resurgent dome in the 5 to 12 km depth range (Steck & Prothero 1994; Sanders & Nixon 1995; Weiland *et al.* 1995). Velocity models based on teleseismic data generally include a volume with anomalously low P-wave velocities somewhere in the 15–30-km depth range beneath the caldera, consistent with a low fraction of partial melt (e.g. Weiland *et al.* 1995), although the sizes, shapes and locations vary from one model to the next. Independent evidence that at least the uppermost 5 km of the resurgent dome is relatively cool and not heated by a laterally extensive, long-lived magma body in the upper 10 km of the crust, comes from: (1) the 100 °C isothermal temperature in the bottom 1 km of the 3-km-deep Long Valley Exploratory Well (LVEW), which is located directly above the centre of inflation on the resurgent dome, and (2) electrical resistivities in excess of 100 Ωm to depths of *c*. 4 km beneath the resurgent dome (Fischer *et al.* 2003; Pribnow *et al.* 2003). These results do not, however, preclude a recent (last 10 000 years, for example) infusion of a small volume (<25 km^3) of magma in the 6- to 7-km depth range beneath the resurgent dome. Thus, although the Long Valley magmatic system may be waning (Hildreth 2004), the recent unrest emphasizes that announcements of its final demise are premature (see Fig. 12).

Evidence on the deeper portion of the Long Valley magmatic system remains sparse. Langbein (2003) suggests that a small difference in the observed deformation field over the SMSZ with respect to that predicted by his prolate ellipsoid model, may be due to a compact inflation source (magma body) in the 10- to 15-km depth range. If real, this deep, but poorly resolved, inflation source may serve as a temporary way-station for magma as it migrates from even greater depths to the shallower magma body beneath the resurgent dome. As yet, however, we see no independent evidence, in the form of deep LP earthquakes or harmonic tremor beneath

the south moat or resurgent dome, that might be associated with active fluid (magma or magmatic brine) transport at depths greater than 10 km.

The mid-crustal LP earthquakes beneath the southwest flank of Mammoth Mountain (Hill & Prejean 2005; Pitt & Hill 1994) presumably coincide with a mid-crustal volume of basaltic magma distributed within a plexus of dykes and sills that underlies the mafic volcanic field surrounding Mammoth Mountain at depths of 10 to 25 km. This magma plexus is likely the source for lavas erupting from the mafic volcanic field, including the *c*. 8 ka basaltic eruptions from Red Cones vents. Mammoth Mountain unrest in the last two decades appears to result from the episodic release of CO_2-rich hydrous fluids from the upper reaches of this magma plexus (Hill & Prejean 2005). The mobilized hydrous fluid induces swarm activity as it ascends through the brittle crust, releasing CO_2 that eventually appears at the surface in areas of diffuse emission through the soil.

The NNE orientation of the seismicity keel activated during the 1989 swarm beneath Mammoth Mountain (Langbein *et al.* 1993; Hill & Prejean 2005), together with focal mechanisms of individual swarm earthquakes, indicates that the extension direction in the vicinity of Mammoth Mountain has a WNW orientation (Figs 9 & 11). The nearly north–south strike of the dyke that fed the Inyo Dome eruptions 500 to 600 years ago implies an east–west extension direction in the vicinity of the Inyo volcanic chain and the west moat of the caldera.

Together, the configuration of these intrusive sources and the stress directions inferred from seismic sources emphasize the spatially heterogeneous nature of active deformation in the vicinity of Long Valley Caldera (Figs 11 & 12). Advances in understanding the tectonic and magmatic processes driving the evolution of this complex volcanic field depend on, among other things, on developing improved images of: (1) the mid-lower-crustal roots to the magmatic system and the deep crustal structure in which this magmatic system resides; and (2) long-term temporal variations in crustal deformation spanning the region including Long Valley Caldera, the White Mountains, the Mono Basin and the northern reaches of the Owens Valley.

Conclusions

The initial and most intense phase of unrest in Long Valley Caldera from 25 May 1980 to 1983 developed with images of the climatic 18 May 1980 Mount St Helens eruption fresh in everyone's mind. The energetic earthquake swarms and pronounced swelling of the resurgent dome within the caldera naturally focused concern on the possibility of a major eruption, fed by what – at the time – was thought to be a sizeable residual of the 760-ka magma chamber. Although few believed that another massive (*c*. 600-km^3), caldera-forming eruption was likely, many considered a major (5- to 10-km^3), explosive eruption a sobering possibility (Miller *et al.* 1982). Perceptions of the volcanic hazards posed by the ongoing unrest evolved rapidly with time, however, as we learned more about the nature of the greater Long Valley–Mono Domes magmatic system through ongoing research. These advances in understanding derived directly from data collected during the evolving unrest, as well as from advances within the volcanological community in understanding restless calderas elsewhere in the world (e.g. Newhall & Dzurisin 1988). As is now clear from the collective experience gained since *c*. 1980, large silicic calderas may exhibit sustained periods of episodic unrest, separated by years to decades of relative quiescence, all without producing an eruption. It is also clear that the more energetic episodes of caldera unrest may significantly exceed the unrest precursory to eruptions of most central-vent volcanoes, in both intensity and duration. A remaining challenge involves developing ever more reliable criteria for early recognition of an escalating unrest episode that portends an eruption from the many that do not.

In the case of Long Valley Caldera, interdisciplinary studies indicate that a laterally extensive, upper-crustal magma body capable of feeding a major eruption does not currently underlie the caldera. These studies do indicate, however, that the 1978–2004 unrest is associated with the addition of *c*. 0.3 km^3 of material (probably a combination of magma and hydrous fluids) at a depth of 6 to 7 km beneath the resurgent dome. Although the size and configuration of a magma body at this depth remains elusive, seismic tomography studies using local earthquake sources would have detected a magma body with a diameter much greater than 1–2 km. This leaves the possibility that a future episode of accelerating caldera unrest could culminate in a small to moderate magmatic eruption (erupted volume < 1 km^3) or series of phreatic explosions from the resurgent dome or south-moat seismic zone (SMSZ).

Although the dacitic magma chamber that fed the Mammoth Mountain eruptions has likely crystallized since the last eruption at *c*. 57 ka (Hildreth 2004), the unrest beneath Mammoth Mountain, including the 1989 earthquake

swarm, mid-crustal LP earthquakes, and CO_2 venting, indicates that the mid-crustal plexus of basaltic magma remains capable of feeding future mafic eruptions (Hill & Prejean 2005). This magma plexus presumably fed eruptions of the mafic field surrounding Mammoth Mountain, including the 8-ka Red Cones vents, and it is the likely heat source for the *c*. 700 a BP phreatic explosion vents on the northeast flank of Mammoth Mountain.

Based on the geological record alone, however, the most likely site for a future eruption in the Long Valley Caldera–Mono Domes volcanic field is somewhere along the Mono–Inyo volcanic chain, which has produced some 20 eruptions over the last 5000 years at intervals ranging from 200 to 700 years, with the most recent eruption from Paoha Island in Mono Lake just 200–300 a BP (Bailey 2004). Aside from occasional mid-crustal LP earthquakes centred some km west of the Mono Domes (Pitt & Hill 1994), however, this system has remained silent during the recent caldera unrest.

Just where and when the next eruption might occur within the Long Valley–Mono Domes volcanic field remains to be seen. As emphasized during discussions resulting from a 2003 workshop on volcanic processes beneath the Long Valley Caldera–Mono Domes area (Hill & Segall 2004), progress in addressing this question depends on developing improved images of the roots to the waning Long Valley caldera magma system, the Mammoth Mountain mafic field and the Mono–Inyo volcanic chain, as well as a better understanding of the modulating influence of regional tectonism on this distributed magmatic complex.

I am grateful to D. Oppenheimer, G. Waite, C. Chiarabba and an anonymous reviewer for their constructive comments on earlier versions of this paper.

References

Bailey, R. A. 2004. *Eruptive history and chemical evolution of the precaldera and postcaldera basalt–dacite sequences, Long Valley, California: implications for magma sources, current magmatic unrest, and future volcanism*. US Geological Survey Professional Papers, **1692**, Reston, VA, US Geological Survey.

Bailey, R. A., Dalrymple, G. B. & Lanphere, M. A. 1976. Volcanism, structure, and geochronology of Long Valley Caldera, Mono County, California. *Journal of Geophysical Research*, **81**, 725–744.

Battaglia, M. & Vasco, D. W. (2006), The search for magma reservoirs in Long Valley Caldera: single versus distributed sources. *In:* De Natale, G., Troise, C., & Kilburn, C. R. J. (eds) *Mechanisms of Activity and Unrest at Large Calderas*. Geological Society, London, Special Publications, **269**, 25–45.

Battaglia, M., Segall, P. & Roberts, C. 2003. The mechanics of unrest at Long Valley Caldera, California: 2. Constraining the nature of the source using geodetic and micro-gravity data. *Journal of Volcanology and Geothermal Research*, **127**, 219–245.

Bursik, M. I. & Sieh, K. E. 1989. Range front faulting and volcanism in the Mono Basin, eastern California. *Journal of Geophysical Research*, **94**(B11), 15 587–15 609.

Bursik, M. I., Renshaw, C., McCalpin, J. & Berry, M. 2003. A volcanotectonic cascade: activation of range front faulting and eruptions by dike intrusion, Mono Basin–Long Valley Caldera, California. *Journal of Geophysical Research*, **108**, doi:10.1029/2002JB002032.

Chouet, B. & Julian, B. R. 1985. Dynamics of an expanding fluid filled crack. *Journal of Geophysical Research*, **90**, 11 187–11 198.

Cramer, C. H. & Toppozada, T. R. 1980. A seismological study of the May, 1980, and earlier earthquake activity near Mammoth Lakes, California. *In:* Sherburne, R. W. (ed.) *Mammoth Lakes, California earthquakes of May 1980*. California Division of Mines and Geology Special Reports, **150**, 91–122.

Dawson, P. B., Evans, J. R. & Iyer, H. M. 1990. Teleseismic tomography of the compressional wave velocity structure beneath the Long Valley region, California. *Journal of Geophysical Research*, **95**, 11 021–11 050.

De Natale, G., Pingue, F., Allard, P. & Zollo, A. 1991. Geophysical and geochemical modelling of the 1982–1984 unrest phenomena at Campi Flegrei Caldera (southern Italy). *Journal of Volcanology and Geothermal Research*, **48**, 199–222.

Dixon, T. H., Miller, M., Farina, F., Wang, H. & Johnson, D. 2000. Present-day motion of the Sierra Nevada block and some tectonic implications for the Basin and Range province, North America. *Tectonics*, **19**, 1–24.

Dreger, D. S., Tkalcic, H. & Johnston, M. 2000. Dilational process accompanying earthquakes in the Long Valley caldera. *Science*, **288**, 122–125.

Ellsworth, W. L. 1990. Earthquake history, 1769–1989. *In:* Wallace, R. E. (ed.) *The San Andreas Fault System, California*. US Geological Survey, Washington DC, 153–187.

Farrar, C. D., Sorey, M. L., *et al.* 1995. Forest-killing diffuse CO_2 emission at Mammoth Mountain as a sign of magmatic unrest. *Nature*, **376**, 675–678.

Fischer, M., Roller, K., Muser, M., Stockhert, B. & McConnell, V. S. 2003. Open fissure mineralization at 2600 m depth in Long Valley Exploratory Well (California) – insight into the history of the hydrothermal system. *Journal of Volcanology and Geothermal Research*, **127**, 347–363.

Foulger, G. R., Julian, B. R., Hill, D. P., Pitt, A. M., Malin, P. E. & Shalev, E. 2004. Non-double-couple microearthquakes at Long Valley caldera, California, provide evidence for hydraulic

fracturing. *Journal of Volcanology and Geothermal Research*, **132**, 45–71.

FOULGER, G. R., MALIN, P. E., SHALEV, E., JULIAN, B. R. & HILL, D. P. 1998. Seismic monitoring and activity increase in California caldera. *EOS, Transactions, American Geophysical Union*, **79**, 357–363.

FOURNIER, R. O. 1999. Hydrothermal processes related to movement of fluid from plastic to brittle rock in the magmatic-epithermal environment. *Economic Geology*, **94**, 1193–1211.

HILDRETH, W. 2004. Volcanological perspectives on Long Valley, Mammoth Mountain, and Mono Craters: several contiguous but discrete systems. *Journal of Volcanology and Geothermal Research*, **136**, 169–198.

HILL, D. P. 1998. 1998 SSA Meeting – Presidential Address: science, geologic hazards, and the public in a large restless caldera. *Seismological Research Letters*, **69**, 400–404.

HILL, D. P. & PREJEAN, S. 2005. Volcanic unrest beneath Mammoth Mountain, California. *Journal of Volcanology and Geothermal Research*, **146**, 257–283.

HILL, D. P. & SEGALL, P. 2004. Interdisciplinary discussion of volcanic processes beneath the Long Valley Caldera–Mono Craters area. *EOS, Transactions, American Geophysical Union*, **85**, 228–230.

HILL, D. P., BAILEY, R. A. & RYALL, A. S. 1985. Active tectonic and magmatic processes beneath Long Valley Caldera, eastern California; an overview. *Journal of Geophysical Research*, **90**, 11 111–11 120.

HILL, D. P., DZURISIN, D., *et al.* 2002*a*. Response plan for volcanic hazards in the Long Valley caldera and Mono Craters area, California. *US Geological Survey Bulletin*, **2185**, 1–57.

HILL, D. P., LANGBEIN, J. O. & PREJEAN, S. 2003. Relations between seismicity and deformation during unrest in Long Valley Caldera, California, from 1995 through 1999. *Journal of Volcanology and Geothermal Research*, **127**, 175–193.

HILL, D. P., POLLITZ, F. & NEWHALL, C. 2002*b*. Earthquake–volcano interactions. *Physics Today*, **55**, 41–47.

HOUGH, S. E., DOLLAR, R. S. & JOHNSON, P. 2000. The 1998 earthquake sequence south of Long Valley caldera, California: hints of magmatic involvement. *Bulletin of the Seismological Society of America*, **90**, 752–763.

JOHNSTON, M. J. S., PREJEAN, S. & HILL, D. P. 2004. Triggered deformation and seismic activity in Long Valley Caldera by the November 3, 2002, M 7.9 Denali Fault Earthquake. *Bulletin of the Seismological Society of America*, **94**, 5360–5369.

JULIAN, B. R. & SIPKIN, S. A. 1985. Earthquake processes in the Long Valley Caldera area, California. *Journal of Geophysical Research*, **90**, 11 155–11 169.

KISSLING, E. 1988. Geotomography with local earthquake data. *Reviews of Geophysics*, **26**, 659–698.

LANGBEIN, J. O. 1989. Deformation of the Long Valley Caldera, eastern California, from mid-1983 to mid-1988; measurements using a two-color geodimeter. *Journal of Geophysical Research*, **94**(B4), 3833–3849.

LANGBEIN, J. O. 2003. Deformation of the Long Valley Caldera, California: inferences from measurements from 1988 to 2001. *Journal of Volcanology and Geothermal Research*, **127**, 247–267.

LANGBEIN, J. O., HILL, D. P., PARKER, T. N. & WILKINSON, S. K. 1993. An episode of reinflation of the Long Valley Caldera, eastern California: 1989–1991. *Journal of Geophysical Research*, **98**(B9), 15 851–15 870.

MCGEE, K. A., GERLACH, T. M., KESSLER, R. & DOUKAS, M. P. 2000. Geochemical evidence for a magmatic CO_2 degassing event at Mammoth Mountain, California, September–December 1997. *Journal of Geophysical Research*, **105**(B4), 8447–8456.

MILLER, C. D. 1985. Holocene eruptions at the Inyo volcanic chain, California; implications for possible eruptions in Long Valley Caldera. *Geology*, **13**, 14–17.

MILLER, C. D., CRANDELL, D. R., MULLINEAUX, D. R., HOBLITT, R. P. & BAILEY, R. A. 1982. *Potential volcanic hazards in the Long Valley Mono Lake area, east central California and southwestern Nevada – a preliminary assessment*. US Geological Survey Circular, 877.

NEWHALL, C. G. & DZURISIN, D. 1988. *Historical unrest at large calderas of the world, Volumes 1 and 2*. US Geological Survey Bulletin, **1855**.

NEWMAN, A. V., DIXON, T. H. & GOURMETEN, N. 2006. A four-dimensional viscoelastic deformation model for the Long Valley Caldera, California, between 1995 and 2000. *Journal of Volcanology & Geothermal Research*, **150**, 214–269.

PITT, A. M. & HILL, D. P. 1994. Long-period earthquakes in the Long Valley Caldera region, eastern California. *Geophysical Research Letters*, **21**, 1679–1682.

PREJEAN, S. 2002. *The interaction of tectonic and magmatic processes in the Long Valley Caldera, California*. PhD thesis, Stamford University, Stamford CA.

PREJEAN, S., ELLSWORTH, W., ZOBACK, M. & WALHOUSER, F. 2002. Fault structure and kinematics of the Long Valley Caldera region, California, revealed by high-accuracy earthquake hypocenters and focal mechanism stress inversion. *Journal of Geophysical Research*, **107**(B12), 2355, doi:10.1029 JB001168.

PREJEAN, S., HILL, D. P. *ET AL.* 2004. Observations of remotely triggered seismicity on the United States west coast following the M7.9 Denali Fault earthquake. *Bulletin of the Seismological Society of America*, **94**, 5348–5359.

PREJEAN, S., STORK, A., ELLSWORTH, W., HILL, D. & JULIAN, B. 2003. High precision earthquake locations reveal seismogenic structures within Mammoth Mountain, California. *Geophysical Research Letters*, **30**, doi:10.1029/2003GL018334.

PRIBNOW, D. F. C., SCHUTZE, C., HURTER, S. J., FLECHSIG, C. & SASS, J. H. 2003. Fluid flow in the resurgent dome of Long Valley Caldera: implications from thermal data and deep electrical sounding. *Journal of Volcanology and Geothermal Research*, **127**, 329–345.

Priestley, K. F., Smith, K. D. & Cockerham, R. S. 1988. The 1984 Round Valley, California earthquake sequence. *Geophysical Journal of the Royal Astronomical Society*, **95**, 215–235.

Roeloffs, E., Sneed, M., Galloway, D. L., Sorey, M. L., Farrar, C. D., Howle, J. F. & Hughes, J. 2003. Water-level changes induced by local and distant earthquakes at Long Valley caldera, California. *Journal of Volcanology and Geothermal Research*, **127**, 269–303.

Sanders, C. O. & Nixon, L. D. 1995. S-wave attenuation in Long Valley Caldera, California, from three component S- to P amplitude radio data. *Journal of Geophysical Research*, **100**, 12 395–12 404.

Savage, J. C. 1988. Principal component analysis of geodetically measured deformation in Long Valley Caldera, eastern California, 1983–1987. *Journal of Geophysical Research*, **93**(B11), 13 297–13 305.

Savage, J. C. & Clark, M. M. 1982. Magmatic resurgence in Long Valley Caldera, California; possible cause of the 1980 Mammoth Lakes earthquakes. *Science*, **217**, 531–533.

Savage, J. C. & Cockerham, R. S. 1984. Earthquake swarm in Long Valley Caldera, California, January 1983; evidence for dike inflation. *Journal of Geophysical Research*, **89**, 8315–8324.

Shapiro, S. A., Audigane, P. & Royer, J-J. 1999. Large-scale *in situ* permeability tensor of rock from induced microseismicity. *Geophysical. Journal International*, **137**, 207–213.

Smith, K. D. & Priestley, K. F. 1988. The foreshock sequence of the 1986 Chalfant, California, earthquake. *Bulletin of the Seismological Society of America*, **78**, 172–187.

Smith, R. B. & Braile, L. W. 1994. The Yellowstone hotspot. *Journal of Volcanology and Geothermal Research*, **61**, 121–187.

Sorey, M. L., Evans, W. C., Kennedy, B. M., Farrar, C. D., Hainsworth, L. J. & Hausback, B. 1998. Carbon dioxide and helium emissions from a reservoir of magmatic gas beneath Mammoth Mountain, California. *Journal of Geophysical Research*, **103**(B7), 15 303–15 323.

Sorey, M. L., Kennedy, B. M., Evans, W. C., Farrar, C. D. & Suemnicht, G. A. 1993. Helium isotope and gas discharge variations associated with crustal unrest in Long Valley Caldera, California, 1989–1992. *Journal of Geophysical Research*, **98**(B9), 15 871–15 890.

Steck, L. K. & Prothero, W. A. Jr, 1994 Crustal structure beneath Long Valley Caldera from modeling of teleseismic P-wave polarizations and S–P converted phases. *Journal of Geophysical Research*, **99**, 6881–6898.

Thatcher, W. & Massonnet, D. 1997. Crustal deformation of Long Valley Caldera, eastern California, 1992–1996, inferred from satellite radar interferometry. *Geophysical Research Letters*, **24**, 2519–2522.

Tryggvason, A., Benz, H. M. & Rognvaldsson, S. T. 1998. Seismic travel time tomography studies of two volcanoes, the Long Valley Caldera, California, and the Hengill Volcano, Iceland [abs.]. *Annales Geophysicae*, **16**, 174.

Van Wormer, J. D. & Ryall, A. S. 1980. Sierra Nevada–Great Basin boundary zone: earthquake hazards related to structure, active tectonic processes, and anomalous patterns of earthquake occurrence. *Bulletin of the Seismological Society of America*, **70**, 1557–1572.

Waldhauser, F. & Ellsworth, W. L. 2000. A double-difference hypocenter algorithm: Method and application to the northern Hayward fault, California. *Journal of Geophysical Research*, **107**, doi:10.1029/2001JB000084.

Wallace, T. C., Given, J. & Kanamori, H. 1982. A discrepancy between long and short period mechanisms of earthquakes near the Long Valley Caldera. *Geophysical Research Letters*, **9**, 1131–1134.

Weiland, C. M., Steck, L. K., Dawson, P. B. & Korneev, V. A. 1995. Nonlinear teleseismic tomography at Long Valley Caldera, using three-dimensional minimum travel time ray tracing. *Journal of Geophysical Research*, **100**(B10), 20 379–20 390.